Thesis

Delivering Functional Cargos by Extracellular Vesicles Engineered with a Lipid-binding Domain

(脂質結合ドメインを用いた人工改変細胞外小胞による機能的カーゴの送達)

March 25th, 2024

Hokkaido University

OPADELE Abayomi Emmanuel

Thesis

Delivering Functional Cargos by Extracellular Vesicles Engineered with a Lipid-binding Domain

(脂質結合ドメインを用いた人工改変細胞外小胞による機能的カーゴの送達)

March 25th, 2024

Hokkaido University

OPADELE Abayomi Emmanuel

Table of Contents

List of Publications and Presentations

Publication

1| Abayomi Emmanuel Opadele, Soichiro Nishioka, Ping-Hsiu Wu, Quynh-Thu Le, Hiroki Shirato, Jin-Min Nam, and Yasuhito Onodera.

A lipid-binding domain D4 of perfringolysin O facilitates the active loading of exogenous cargo into extracellular vesicles.

FEBS Letters, (Accepted for Publication on December 15, 2023)

DOI: 10.1002/1873-3468.14807

Status: In Production

Presentation

1| Abayomi Emmanuel Opadele, Soichiro Nishioka, Ping-Hsiu Wu, Hiroki Shirato, Jin-Min Nam, and Yasuhito Onodera.

D4 facilitates active cargo recruitment into EV.

The 10th Annual Meeting of the Japanese Society for Extracellular Vesicles.

October 23rd, 2023. Sapporo, Japan (Poster presentation)

Abstract

Extracellular vesicles (EVs) contain complex cargos that regulate cellular and phenotypic changes in recipients' cells. EV inherent structures also make them a viable platform for drug delivery in biomedicine. Tetraspanins protein such as CD9 and others have served as a customary molecular machinery for loading foreign cargos into EVs, however the overexpression of CD9 in EV is believed to affect precise cellular targeting and could also promote viral entry into recipient cells. To develop an alternative loading and delivery system for EV cargo, we report Domain 4 (D4), a lipid-binding domain derived from a bacterial protein of perfringolysin, as a viable platform for the efficient loading of proteins of interest (POIs) into EV. To validate the efficacy of D4-EVs, we compared its loading efficiency and protein delivery capacity relative to that of widely-utilized CD9-EVs. Our results suggests that D4 enables successful intracellular EV cargo release and content release was enhanced with the aid of vesicular stomatitis virus glycoprotein (VSV-G).

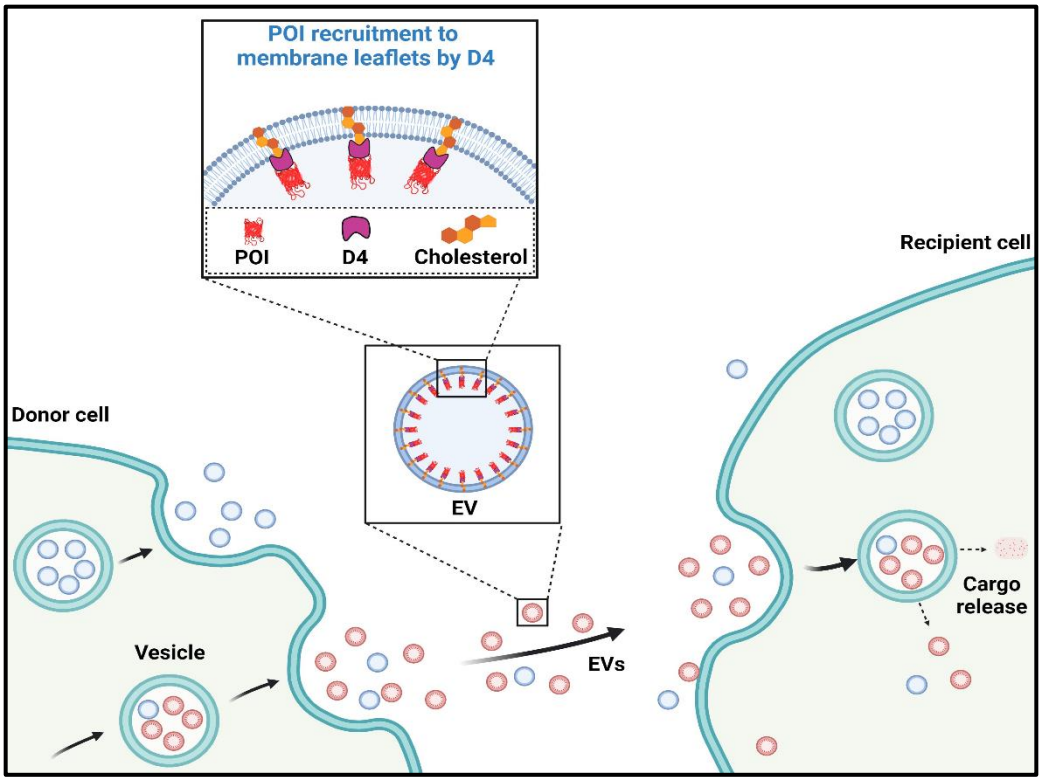

Fig I: Overall schematics of this study

[Background]

Custom-designed drug delivery vehicles for biomedical applications now predominantly involve the use of extracellular vesicles (EVs) as opposed to viral vectors. EVs represent an array of membrane-enclosed vesicles secreted by both eukaryotic and prokaryotic cells, containing diverse cargos including DNA, RNA, proteins, lipids, and metabolites. EVs distinctive features make them an attractive candidate for intracellular and targeted protein delivery. Tetraspanins proteins (CD9, CD63 and CD81) and other EV-localizing proteins such as PTGRFN and BASP1 are widely used proteins for loading exogenous bioactive molecules into EVs, however tetraspanin-enriched EVs may affect cell targeting due to their inherent fusogenic abilities. In this thesis, we report an alternative platform for recruiting protein of interests (POIs) into EVs through a lipid-binding domain 4 (D4). We studied the efficiencies of D4 for EV loading and for intracellular protein delivery.

[Methods and Results]

1| We constructed plasmid vectors expressing several fusion proteins such as TagRFP, FusionRedMQV (FRMQV) and mScarlet-I as models for POI and individually fused them to EV sorting proteins to generate CD9-POI, D4H-POI, D4-YDA-POI, and D4-YQDA-POI.

2| We evaluated the protein expression and intracellular localization of these plasmid vectors after transient and stable transfection in various cell lines. D4 efficiently recruits POI into EVs and shows localization to plasma membrane (PM) and vesicular structures in cell cytosol.

3| We increased the affinity of D4 to cholesterol by introducing additional mutants into D4. Accumulation of D4 mutants was expressed in EVs and localizes to plasma membrane of cells.

4| Through immunoblotting, we determined the loading efficiency of POI between D4 and CD9 and confirm that D4 loads POI with analogous efficiency as CD9.

5| Through confocal live imaging, we showed that D4-EVs are internalized by recipient cells and are functional in cell's cytosol.

6| Lastly with the aid of split-luciferase technology and fusogenic proteins, our analysis shows that D4-EVs are capable of intracellular protein delivery in recipient cells.

[Discussion]

In this thesis, we describe how a lipid-binding domain (D4) derived from bacterial protein, *Clostridium perfringens* can be utilized as an active platform for loading exogenous cargo into EVs.

1| D4 have been previously reported to mediate cholesterol recognition and membrane binding. Since EVs are also enriched in cholesterol, we harnessed D4 binding affinity to cholesterol to facilitate engineering of EV cargo. Further studies are required to optimize D4's affinity to cholesterol for enhancing and regulating the loading of POI into EVs.

2| The uptake efficiency of D4-EVs was higher when compared with CD9-EVs. Additionally, the efficiency of intracellular protein delivery between CD9 and D4 are almost equivalent when assisted with VSV-G. This demonstrates that D4-EVs mediates efficient protein delivery and further studies are required to investigate the effect of small molecule inhibitors and enhancers on the cargo delivery of D4-EVs.

[Conclusion]

Conclusively, **we report for the first time the role that D4 plays in engineering of EVs**. Our results shows that fluorescent and luminescent reporters can be loaded into EVs through D4 and achieve equivalent loading efficiency with widely used CD9. The outcome of this research has the potential to open a new vista of exploration for studying cell-cell communication through D4 engineered EVs.

List of Abbreviations

Abbreviation	Full meaning
ARRDC1	Arrestin domain-containing protein 1
BSA	Bovine serum albumin
CCK-8	Cell counting kit-8
CD9	Cluster of Differentiation 9
CDC	Cholesterol-dependent cytolysin
CM	Conditioned medium
CPP	Cell penetrating peptide
CRISPR	Clustered regularly interspaced short palindromic repeat
D4	Domain 4
D4H	Domain 4 with higher affinity
DAPI	4’,6-diamino-2-phenylindole
DMEM	Dulbecco’s Eagle’s Medium-High Glucose
DNA	Deoxyribonucleic
Dox	Doxycycline
DrkBiT	DarkBiT
EdFBS	Exosome depleted fetal bovine serum
EDTA	Ethylenediaminetetraacetic acid
EEA1	Early endosome antigen 1
EMEM	Minimum Essential Medium Eagle
ESCRT	Endosomal sorting complex required for transport
eTEVp	Enhanced tobacco etch virus protease
EV	Extracellular vesicles
EVCD	Extracellular vesicles cargo delivery
FBS	Fetal bovine serum
FP	Fluorescent protein
FRMQV	Fusion red MQV
GFP	Green fluorescent protein
HiBiT	Small bit with high affinity
ILV	Intraluminal vesicle
LAMP2A	Lysosome-associated membrane protein 2, isoform A
LDL	Low-density lipoprotein
LDS	Lithium dodecyl sulfate
LgBiT	Large bit
MVB	Multivesicular body

Nluc	Nanoluciferase
PAC	Puromycin N-acetyltransferase
PBS	Phosphate buffered saline
PCA	Protein fragment complementation assay
PCR	Polymerase chain reaction
PEG	Polyethylene Glycol
PFA	Paraformaldehyde
PFO	Perfringolysin O
PM	Plasma membrane
POI	Protein of Interest
PVDF	Polyvinylidene fluoride
RFP	Red fluorescent protein
RIPA	Radioimmunoprecipitation assay
RNA	Ribonucleic acid
SDS	Sodium dodecyl sulphate
SEC	Size exclusion chromatography
sgRNA	single guide RNA
SmBiT	Small bit
TagRFP	Tag Red fluorescent protein
TEV	Tobacco etch virus
VLP	Virus like particles
VSV-G	Vesicular stomatitis virus glycoprotein

List of Figures

Introduction

Brief history of EVs

Extracellular vesicles (EVs) have gained prominence in the field of cell biology and attracting attention in recent years as delivery vehicles carrying diverse array of cargos (Fig II). The earliest evidence of EVs dates to 1946, when Chargaff et al., discovered that a platelet-free plasma fraction retained clotting properties and was fractionated into a coagulatory pellet after high-speed ultracentrifugation (CHARGAFF & WEST, 1946). In early 1980s, reports emerged highlighting the ability of tumour cells to produce these 'pelleted-particles' (H. F. Dvorak et al., 1981; Harold F. Dvorak et al., 1983). It wasn't until 1987, during investigations into reticulocyte maturation, that Johnstone et al., introduced the term "exosomes" to describe these particles (Johnstone, Adam, Hammond, Orr, & Turbide, 1987). Initially exosomes were considered cellular waste containers, but they re-gained significance in 1998 when Zitvogel et al., proposed their involvement in intercellular communication among immune cells, solidifying their role as mediators of cell-cell communication (Zitvogel L, Regnault A, Lozier A, Wolfers J, Flament C, Tenza D, Ricciardi-Castagnoli P, Raposo G et al., 1998). Afterwards, several groups began to investigate the composition, characterization, and proteome of EVs as well as their effects on neighbouring cells. This led to a prominent discovery that EVs contains genetic materials and can horizontally transfer RNA and protein cargo to recipient cells (Ratajczak et al., 2006; Skog et al., 2008; Valadi et al., 2007). EVs which are secreted by all cell types and isolated from nearly all biological fluids are classified into – ectosomes and exosomes (Couch et al., 2021; Hoshino et al., 2020; Zhang et al., 2019). For nomenclature purposes, **vesicles as described in this thesis shall be therein referred to as extracellular vesicles (EVs)** (Théry et al., 2018; Witwer et al., 2021).

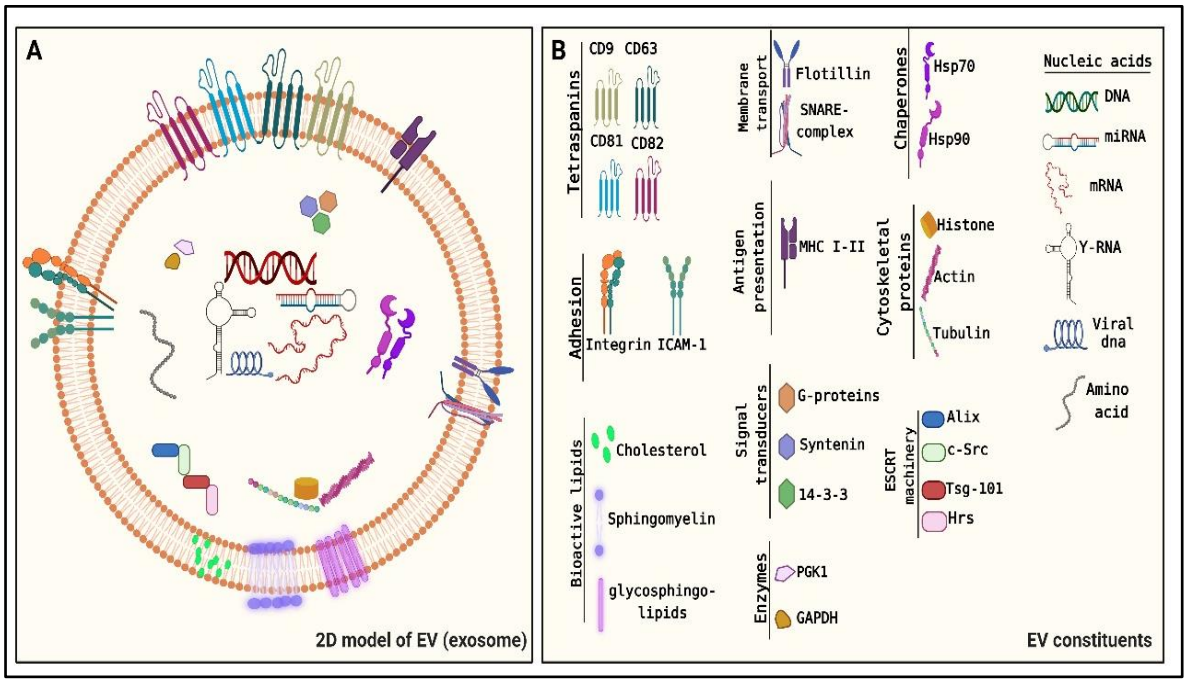

Fig II: A schematic model of the biologically active components of extracellular vesicles.

Current challenges involved in EV research

EVs have emerged as customed designed drug delivery vehicles for biomedical applications (Luan et al., 2017; Mehryab et al., 2020). Based on published literatures, EVs have been passively or actively loaded with protein of interests (POIs), diagnostic molecules, and therapeutic agents. While there have been several strategies for developing engineered EVs for horizontal transfer of information to recipient's cells, the functionality of EVs after cellular uptake, process for cargo discharge, and **the cytoplasmic delivery of EV cargos are topics that still require critical elucidation** (Fu, Wang, Xia, & Zheng, 2020a; Somiya, 2020).

A novel tool for engineering of EVs

To unravel one of the challenges previously stated, this thesis focuses on recruiting POIs into engineered EVs and detecting the release of POIs into cytoplasmic environment of recipient cells by utilizing a cholesterol dependent lipid-binding domain 4 (D4) derived from a toxin perfringolysin O (PFO) that is secreted from an anaerobic bacterium *Clostridium perfringens* (Lin & London, 2013; Liu et al., 2017; Maekawa & Fairn, 2015; Ramachandran, Heuck,

Tweten, & Johnson, 2002). **In this study, we shifted our attention to deploy D4 as a platform for recruiting POI into EVs and for assessing efficiency of cargo loading and protein delivery to recipient cells using a split-luciferase technology**. Furthermore, the efficiency of cargo delivery was enhanced by expressing EVs with fusogenic protein - vesicular stomatitis virus glycoprotein (VSV-G) (Meyer et al., 2017). We have demonstrated D4 as a viable candidate for EV-based engineering strategies.

The findings from this study have a single theme and divided into three experimental findings. In experimental finding 1, we investigated the role of D4 in recruiting cargo into EVs and confirmed that D4 localizes to plasma membrane and vesicular structure in cell's cytosol. In this section, we loaded TagRFP as a model of POI into EVs. In experimental finding 2, we analysed the uptake and loading efficiency of D4 and compared with widely used CD9, and we utilized mScarlet-I as a model of POI. In experimental finding 3, we describe using split-luciferase technology to intracellularly deliver D4-EVs into the cytoplasmic environment of recipient cells, while using HiBiT peptide as a model of POI.

Experimental Finding 1.

Investigating the role of D4 in recruiting protein cargo into EV

1.0 Brief Introduction

Within the plasma membrane (PM) of mammalian cells, a wide range of lipid molecules exhibit diverse structural and functional characteristics (Murate & Kobayashi, 2016; van Meer, 2011). One prominent lipid, cholesterol, assumes a vital role in the PM by contributing to its structural integrity and fulfilling essential functional roles such as permeability, thickness, and fluidity (Johnson, Breña, Anguita, & Heuck, 2017; Maxfield & van Meer, 2010). Cholesterol is derived from two main pathways in mammalian cells: 1) through de novo biosynthesis in the endoplasmic reticulum and 2) from low-density lipoprotein (LDL) receptor-mediated endocytosis ensuing hydrolysis in lysosomes (Mesmin & Maxfield, 2009). Cholesterol is an amphipathic molecule containing hydrophilic and hydrophobic sections, its entire structure is characterized by a hydrophobic sterol of four hydrocarbons and one hydroxyl group as a polar head, i.e. one hydrogen atom bonded to one oxygen atom (Kumar & Chattopadhyay, 2016; Maekawa, 2017). The hydroxyl group aligns with the phosphate head of the cell membrane's phospholipid, while the remaining portion (*non-polar head*, *hydrocarbon tail)* associates with the membrane's fatty acid (Fig 1.0.1).

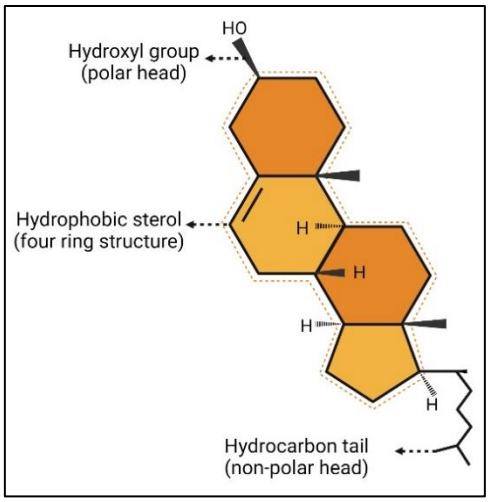

Fig 1.0.1: Chemical structure of cholesterol. The cholesterol is a four rigid ring structure consisting of a hydroxyl group and a hydrocarbon tail. The polar head attaches to the membrane lipid layer while the non-polar head associates with membrane's fatty acid.

The concentrations of cholesterol in PM are tightly regulated and few studies have demonstrated the possibilities of quantifying the varying cholesterol levels in PM through a lipid-binding cholesterol-dependent cytolysin (CDC) (Liu et al., 2017).

Several toxins have been reported to play specific roles in membrane synthesis through the cholesterol-enriched sites within the PM. The perfringolysin O (PFO) derived from spore-forming Gram-positive bacteria *Clostridium perfringes* is a peculiar toxin that recognizes and binds with cellular membrane through cholesterol (Verherstraeten et al., 2015). PFO belongs to the CDC family and consists of four different structural domains (Fig 1.0.2).

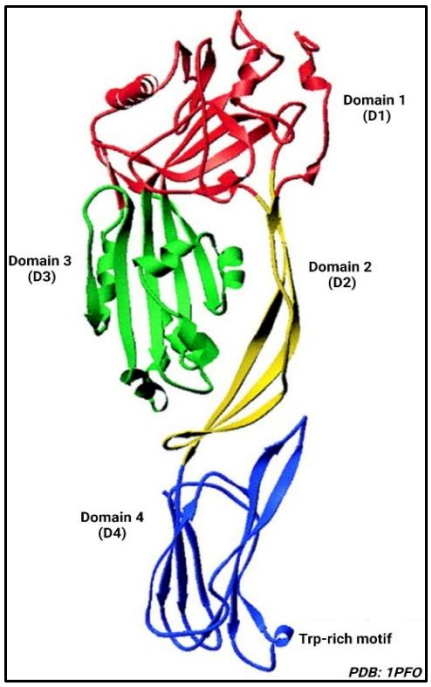

Fig 1.0.2: Structural domains of PFO molecule. The PFO consists of four domains. D4 possesses no toxicity and recognizes the hydroxyl group of cholesterol and mediates plasma membrane binding *(Image extracted from www.rcsb.org, ID = 1PFO).*

Studies have shown that domain 4 (D4) mediates recognition and binding to cholesterol at the PM (Ramachandran et al., 2002). While D4 serves as the membrane insertion domain with no cytotoxic effect to PM (Shimada, Maruya, Iwashita, & Ohno-Iwashita, 2002), D4 with a point mutation (D434S), named D4H (D4 with higher affinity) has also been reported to significantly lower threshold for cholesterol (Johnson et al., 2012; Liu et al., 2017).

Additionally, Liu et al., reports that by introducing several mutations (Y415A, Q433W, D434W and A463W) into D4 will also increase its affinity to cholesterol (Liu et al., 2017). Therefore, cholesterol-rich areas in target cell PM are putative binding sites for D4 and this makes D4 a potential candidate for exogenous protein insertion and loading.

In the past decade, the process of delivering biological genes into eukaryotic cells have been employed using EVs. While EVs are promising nanocarriers for drug-delivery systems, the concept of EV-cargo loading remains poorly characterized. The several strategies for loading POI into EVs have been through the ubiquitously expressed tetraspanins members (CD9, CD63 and CD81). Tetraspanins CD9 are localized on the plasma membrane, and they facilitate numerous biological events such as cell adhesion, motility, inducing tumor progression and immune response (Hemler, 2005). Some major drawbacks of engineering CD9 for loading POI into EVs are: 1) tetraspanins EVs may affect cell targeting due to inherent fusogenic abilities (Hemler, 2003). 2) CD9 are reported to be involved in viral-infectivity such as HIV-1 infection (Böker et al., 2018; New et al., 2021), and CD9 overexpression enhances viral entry or syncytia formation in cells (Gordón-Alonso et al., 2006). 3) The high content of CD9 in the engineered EVs may also induce integrin activation of donor cells (Kotha, Longhurst, Appling, & Jennings, 2008) leading to unnecessary recruitment of protein complexes forming focal adhesion sites (Sun, Costell, & Fässler, 2019). Following these drawbacks, it is imperative to develop a suitable strategy for loading POI into EVs. In this report, we focus on the potential of D4 for the cargo loading process.

Since PFO recognizes cholesterol in PM through a tryptophan-rich motif within D4 (Nelson, Johnson, & London, 2008; D. K. O'Brien & Melville, 2004; Shimada et al., 2002), and EVs have been reported to be highly enriched in cholesterol, sphingomyelin, and phospholipids, which is suggestive of the presence of lipid raft-like domains within their membranes (Llorente et al., 2013; Möbius et al., 2003; Skotland, Hessvik, Sandvig, & Llorente, 2019). Owing to this, we selectively chose D4 among other lipid-binding/domains for recruiting POIs into EVs. In some previous studies, cholesterol-binding protein have been used to quantify and probe the transport of cholesterol levels in membranes of animal cells by

labelling mutated form of PFO with Iodine-125 (Das, Goldstein, Anderson, Brown, & Radhakrishnan, 2013). Similarly, D4H have been developed as a genetically encoded biosensor for visualizing cellular distribution of cholesterol in membrane leaflets (Liu et al., 2017; Maekawa & Fairn, 2015). **Up till now, there has been no studies on the utilizing D4H as a recruitment platform for engineering of EV cargos.**

In this section, we actively loaded several variants of red fluorescent proteins namely (TagRFP, Fusion Red MQV[FRMQV], mScarlet-I) as a model of POI for transport into EVs. We evaluated the POIs lysate and EV expressions in several cell types and determined their localization through live cell imaging. Furthermore, we introduced additional mutants (Y415, Q433, A463) to D4H (D434) which are known to increase the affinity of D4 domain to cholesterol and tested their EV accumulation efficiency of POIs (Liu et al., 2017). Finally, we evaluated whether D4-EVs can be captured by CD9-positive EVs to confirm the universality of D4 for EV-engineering purposes.

1.1 Materials and Methods

1.1.1 Molecular cloning and plasmid construction

For the construction of red fluorescent protein (RFP) vectors, CD9, D4H, D4-YDA and D4-YQDA, were inserted into pPB-CEH-MCS-IP together with a series of RFP genes (TagRFP, FRMQV and mScarlet-I). Oligonucleotides used for plasmid construction were synthesized by Integrated DNA technologies. All plasmids were generated by Gibson cloning. DNA modifications were made using KOD (Novagen) and PCR cloning was performed with Taq polymerase (NEB). Plasmids were transformed in heat shock competent *E. coli* and purifications of plasmids were conducted with Qiagen kits according to manufacturer's instructions.

1.1.2 Cell culture and transfection

The cell lines were obtained from American Type Culture Collection (ATCC) and cultured at 37°C in a humidified atmosphere containing 5% CO_2. MDA-MB-231 cells were cultivated in equal volumes of Dulbecco's Eagle's Medium-High Glucose (DMEM, Nacalai Tesque)

and RPMI1640 (Sigma-Aldrich) supplemented with 10% (v/v) Fetal Bovine Serum (FBS, HyClone), and 2 mM L-glutamine. HEK-293T human embryonic kidney cells were maintained in DMEM supplemented with 10% (v/v) FBS. U87-MG cells were cultured in Minimum Essential Medium Eagle (EMEM, Sigma-Aldrich) and supplemented with 10% (v/v) FBS. SNU-449 cells were cultured in RPMI-1640 including 10% FBS. 0.05% trypsin-EDTA (Gibco) was used for serial passaging of HEK-293T, SNU-449 and MDA-MB-231 cells, while U87 cells were trypsinized with 0.25% trypsin-EDTA. To allow for the early detection of mycoplasma contamination, all cell lines were frequently assessed with the Mycoplasma Detection Kit (Lonza) and nuclear staining were performed with DAPI (fixed cells) or Hoechst 33342 (live cells).

1.1.3 Preparation and isolation of EVs

Cells were cultured in respective cell mediums as described above and then replaced with medium containing 10% exosome depleted FBS (bioSera). The conditioned medium (CM) was collected in a sterile tube (1.5 ml Eppendorf tube for 1 ml of CM or 15 ml tube for 5-10 ml of CM) after a minimum of 48 h in culture. Afterwards, cell debris and apoptotic blebs were removed by centrifuging CM at 2,000xg for 30 min and filtered through a 0.22 µm filter (ADVANTEC®). To proceed to isolation of concentrated EVs by precipitation using either Total exosome isolation kit (Invitrogen) or 4XPolyethylene Glycol buffered solution (WAKO). CM was transferred to a sterile tube and mixed with the appropriate volume of reagent buffers (1:2 for Total exosome isolation kit and 1:4 for 4XPEG buffer). Samples were gently pipetted up-down and incubated in 4°C overnight. Centrifugation was performed for the sample mixture (10,000xg for 60 min – Total exosome isolation kit or 3,000xg for 30 min – 4XPEG buffer). After centrifugation the supernatant was carefully aspirated and centrifuged again for 3-5 mins to collect remaining supernatant due to surface tension inside the tube and carefully discarded. EV pellet was concentrated to 100 µl in PBS enriched from 5-10 ml of CM by filtering through a 0.2 µm syringe filter and the resulting pellet was quantified for protein concentration corresponding to the µg of EVs by Bradford (WAKO) or Bio-Rad Protein (Bio-Rad Laboratories) assay according to manufacturer's instruction.

For EV cargo detection by immunoblotting, EV in PBS was sonicated to disrupt the vesicle membrane with BIORUPTOR (Cosmo Bio) and samples were denatured in LDS and mercapethanol buffer and heated at 70°C for 10 min. Classical EV positive or negative markers such as CD9, and GM130 were probed by antibodies respectively.

1.1.4 EV capture by CD9 magnetic beads

To capture CD9-enriched EVs by using ExoCap™ Streptavidin Kit (MBL), cells were seeded for EV isolation as described in the main text. Afterwards, 100 μl of streptavidin magnetic beads slurry mixed with biotinylated anti-CD9 antibody, prepared according to the manufacturer instructions, was transferred to a 1.5 ml tube and placed on a magnetic rack (Tamagawa Seiki) and after a minute the supernatant was carefully removed. At a ratio of 1:1, EV pellet in PBS (50 μl) was mixed with Treatment Buffer (50 μl) and transferred into the previous tube, mixed by inverting the tube and the sample was incubated for up to 24 h in 4°C on a rotating device (AS ONE MTR-103). After incubation, the beads were collected by using the magnetic rack, washed 2 times with 500 μl of Washing Buffer, finally suspended in 500 μl of Dilution Buffer and transferred to a fresh tube. Supernatant was carefully removed by using the magnetic rack, and LDS sample buffer mixed with 2-mercaptoethanol was added directly to the beads. EVs captured on the beads were eluted by incubation at room temperature for 10 min, and EV contents in sample buffer was collected into a new tube, incubated at 70°C for 10 min, and loaded onto polyacrylamide gel for immunoblotting.

1.1.5 Immunoblotting

To perform extraction of proteins, cells were lysed with appropriate volumes of 1% radioimmunoprecipitation assay (RIPA) buffer containing 1% NP-40, 150 mM NaCl, 50 mM Tris-HCl (pH 7.4), 5 mM ethylenediaminetetraacetic acid (EDTA), 1% sodium deoxycholate, 0.1% sodium dodecyl sulfate (SDS), 1 mM Na_3VO_4, 1 mM NaF and protease inhibitor cocktail (Merck Millipore). Twenty μg of proteins samples were resolved by 10% SDS-PAGE or NuPAGE Bis-Tris protein gels (Thermo Fisher Scientific), and then transferred onto polyvinylidene fluoride (PVDF) membrane (Merck Millipore). The membranes were blocked with InterceptTM blocking buffer (LI-COR) at room temperature (RT) for 1 h

followed by incubation with primary antibodies, overnight at 4°C. The membranes were washed three times with Tris-buffered saline containing Tween-20 (TBST; 25 mM; pH 7.4, 120 mM NaCL, 3mM KCl and 0.1% Tween-20) for 10 min each, the membranes were incubated with IRDye secondary antibodies (LI-COR) at RT for 1 h, and then washed with TBST and PBS. Images were acquired with Odyssey Imaging System (LI-COR).

1.1.6 Live cell imaging

To evaluate morphological expression and localization of RFP-fused proteins in HEK-293T cells, 1×10^4cells were seeded on 35mm- glass bottom dish. 12hrs after seeding, cells were replaced with fresh medium supplemented with 2.5 µg/ml Hoechst 33342. Random acquisition of fluorescent images was performed using a Leica TCS SP8 confocal laser scanning microscope, which was equipped with a heater and CO_2 incubator to facilitate live cell imaging. Hoechst 33342 was visualized using a 405nm laser and detected within the spectral range of 410-574nm. RFP visualization, on the other hand, utilized a 552nm laser with spectral detection ranging from 580nm to 755nm.

1.1.7 Fluorescence quantification of EV in conditioned medium

The fluorescent intensity of isolated extracellular vesicles (EVs) derived from the conditioned media (CM) of HEK-293T donor cells, which were seeded in an equivalent number, was quantified. Same volume of CM was transferred to 96-well plates in replicates of 6 samples after centrifugation (2000g, 10min) to remove cell debris. Fluorescence signal was measured by plate reader in a bottom-optic mode with equal RFP settings (Ex 540-20nm, Em = 590-20nm with an autofocus = 565nm and gain = 1500).

1.1.8 Cholesterol depletion by methyl-β-cyclodextrin treatment

Cholesterol depletion using Methyl-β-cyclodextrin (MβCD, FUJIFILM Wako Chemical Corporation) was performed as described previously (Claire McGraw, Lewen Yang, Ilya Levental, Edward Lyman, 2019; Parmryd, 2015). Briefly, MβCD was dissolved in 12.5 mM HEPES buffer, and HEK-293T cells cultured in the exosome-depleted medium for 3 h were

treated with freshly prepared MβCD at final concentrations of 1.25 or 5.0 mM for up to 24 h.

1.1.9 Size exclusion chromatography (SEC)

SEC was performed using MiniPURE-EVs (HansaBioMed Life Sciences) to isolate highly pure EVs. EV-rich and EV-poor fractions were isolated following to the manufacturer's instructions. Briefly, the preservative buffer in the column was removed, followed by a thorough wash with PBS. CM pre-concentrated (10 folds) using Vivaspin Turbo 15 (MWCO 100 kDa PES filter, Sartorius) was loaded onto the column, and 20 fractions were collected in 100 µl PBS each.

1.1.10 Statistical Analysis

Graph shows three independent measurements with mean ± SEM. Statistical analysis was performed using one-way ANOVA adjusted by Tukey's test. ns (not significant) denotes P > 0.05 and *P = 0.00191 (Fig 1.2.2D). While in (Fig 1.2.4B), analysis was performed with two-tailed t-test, *P<0.05, **<0.005 and n.s not statistically significant, $^{\#}$compared to RFP-D4H. Values were normalized to RFP-D4H.

1.2 Results

1.2.1 Topology and recruitment of TagRFP into EV through D4H

To develop a platform for actively loading POIs into EVs through D4H, we fused D4H to an RFP (namely TagRFP), as a model of POI (Fig. 1.2.1). D4H has been previously reported to bind to cholesterol in the exofacial leaflets of cellular membrane (Maekawa, 2017), however, our strategy ensures that D4H recognizes cholesterol domiciled in the highly enriched sites of the EV membrane. This fusion strategy will translate to the recruitment of TagRFP into EV during its biogenesis from multi vesicular bodies (MVB) into extracellular cargo vesicles. (Fig 1.2.1A). To assess the incorporation of RFP into EVs through D4 domain, we transiently transfected four different cell lines namely: HEK-293T, U87MG, MDA-MB-231 and SNU-449 with plasmid vectors encoding TagRFP-D4H constructs. Cell lysates were harvested and EVs were isolated using precipitation method (Fig. 1.2.1B). We compared the protein expression levels of RFP between lysates and EV fractions to determine the loading of POI into EVs by immunoblotting. We confirmed the presence of RFP in EV fractions of all four cell lines, suggesting that D4H successfully loads POI cargo into EVs in various cell types (Fig. 1.2.1 C-F). We found a slight accumulation of RFP-D4H EVs in U87MG glioblastoma cells compared to other cell lines and this may be due to the high cholesterol content in glioblastoma cells (An & Weiss, 2016). To confirm the purity of EV isolation, a negative marker of EV, GM130 was not detected in all EV fractions but only expressed in lysate fractions. Also, CD9 which is highly enriched in EV and serves as a positive marker protein was seen in both lysate and EV fractions of all cell types.

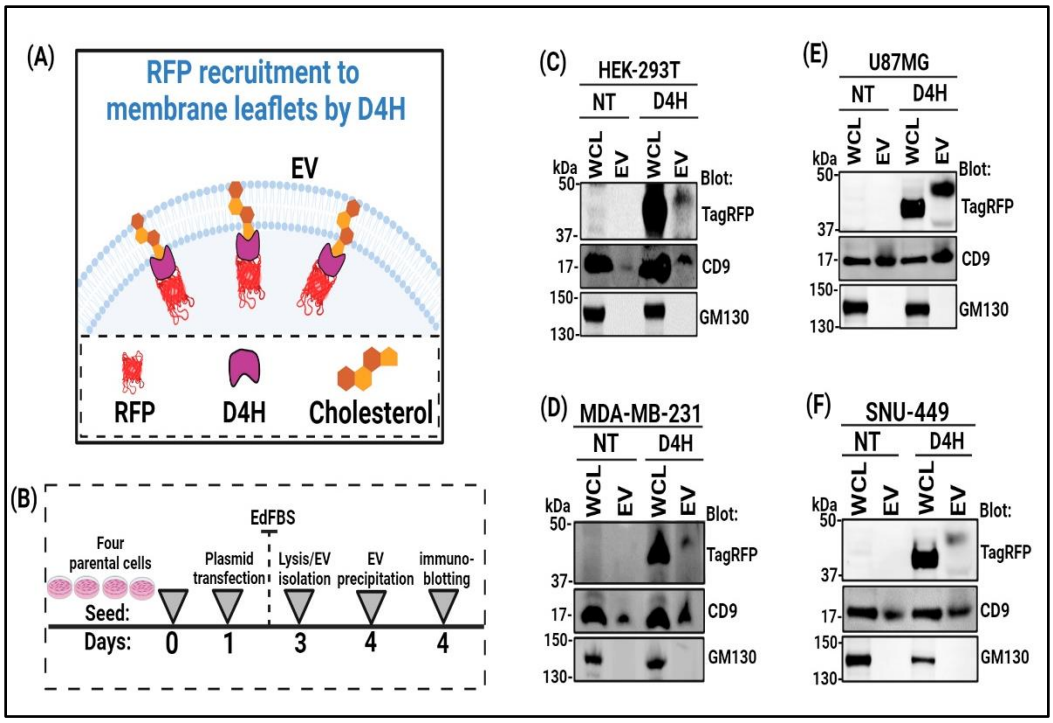

Fig 1.2.1: Characterization of RFP-D4H loaded EVs in several cell lines. (A) A schematic model of how D4H recognizes cholesterol enriched sites in the membrane bilayer of EV and ensures cargo incorporation of TagRFP into EVs. (B) Experimental set-up of transfecting several cell lines for assessing TagRFP expression into EV. Cells were transiently transfected with 2.5ug of RFP-D4H plasmid. (EdFBS, exosome depleted fetal bovine serum). (C-F) Presence of TagRFP-D4H was analysed both in cell lysates and EV fractions in different cell lines, HEK293T (C), MDA-MD-231 (D), U87MG (E), and SNU-449 (F). CD9 and GM130 were used as positive and negative controls for EV fraction, respectively. Non-transfected cells (NT) were also analysed for comparison.

1.2.2 Protein expression of D4 mutant in lysate/EV fractions of HEK293T cells

To increase the affinity of D4 domain to cholesterol, a previous study introduced a point mutation into D4 site for this purpose (Johnson et al., 2012). Following this strategy, we also introduced three additional mutations (Y415A, Q433W and A463W) that are known to enhance D4's affinity to cholesterol (Liu et al., 2017). To generate RFP-$D4_{YDA}$ and RFP-$D4_{YQDA}$, we introduced (Y415A, D434W and A463W mutations) and (Y415A, Q433W, D434W and A463W mutations) respectively (Fig 1.2.2A) and EVs were isolated using

precipitation method (Fig. 1.2.2B). Our result shows that these mutants also accumulate in EV fraction of stable HEK293T cells (Fig. 1.2.2C). D4 domain of PFO has an amino acid length of 117aa which is equivalent to about 13kDa (Maekawa, 2017). Likewise, cytosolic TagRFP is observed at 30kDa. Therefore, the fusion of TagRFP with D4 is expected to be observed at around 43-45kDa. As indicated in our result, a 30kDa band was seen only in the TagRFP lane of the lysate fraction and not in the EV fractions suggesting that TagRFP itself is not recruited into EVs. As expected, we observed that the mutants of D4 fused with TagRFP are expressed around 45kDa in lysate fractions and detected in the EV fractions. Also, there was no statistically significant difference in cargo loading efficiency of D4H-EVs, when compared with $D4_{YDA}$-EVs (Fig 1.2.2D). Altogether, this further confirms that D4 and its mutants indeed transports POIs into EVs.

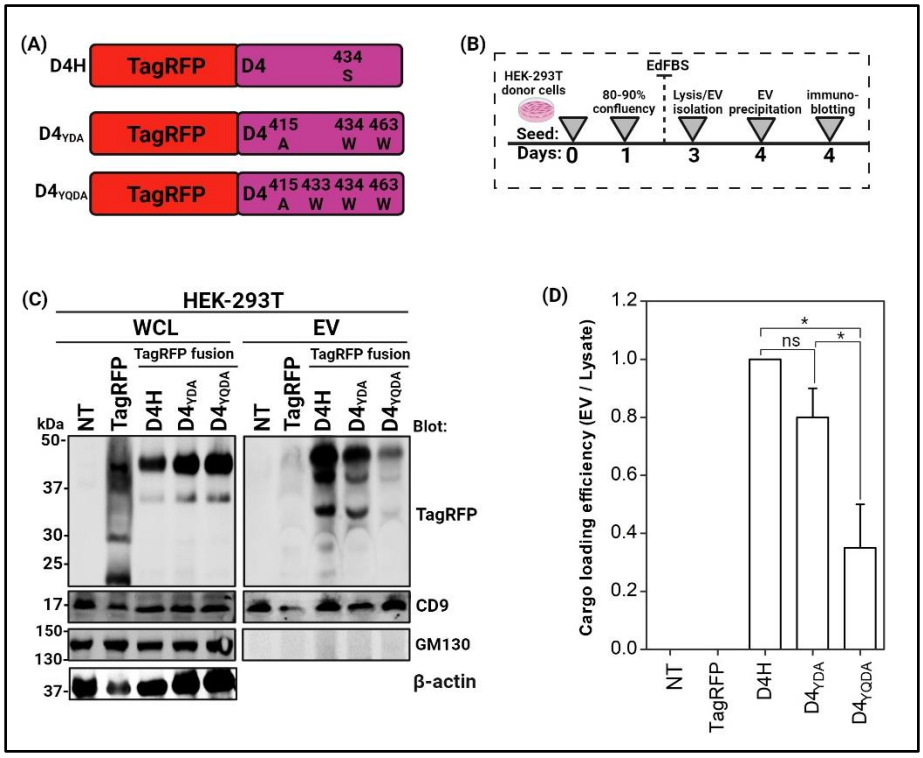

Fig 1.2.2: Construction and detection of D4-mutants loaded into EVs. (A) Schematic representation of amino acid substitution introduced into D4 to generate D4 relatives (D4H, $D4_{YDA}$, $D4_{YQDA}$) (B) Experimental set-up of isolating EVs from HEK-293T donor cells stably expressing construct in (A). Cells were replaced medium containing 10% EdFBS (exosome depleted fetal bovine serum). (C) Cell lysates and EV fractions were subjected to immunoblotting with antibodies, as

indicated. β-actin serves as loading control. (D) Quantification of western blots described in (C). The ratio of TagRFP in EV fraction to lysate was plotted and normalized to D4H. Statistical analysis was performed using ANOVA adjusted by Tukey's test. ns (not significant) denotes P > 0.05 and *P = 0.00191. Graph shows mean ± SEM from two different experiments.

1.2.3 Cellular localization of TagRFP-D4H variants in HEK-293T cells

To evaluate the localization of each TagRFP-D4 series, HEK293T cells stable expressing the RFP-tagged proteins were subjected to live imaging by confocal microscopy. The microscopic images show that RFP-D4H and it variants localizes to intracellular vesicle like structures and in PM, while RFP-CD9 mainly localized to PM (Fig. 1.2.3). The presence of RFP-D4H in vesicles is likely due to D4 domains binding to cholesterol in the lipid leaflets after their translation in cytosol.

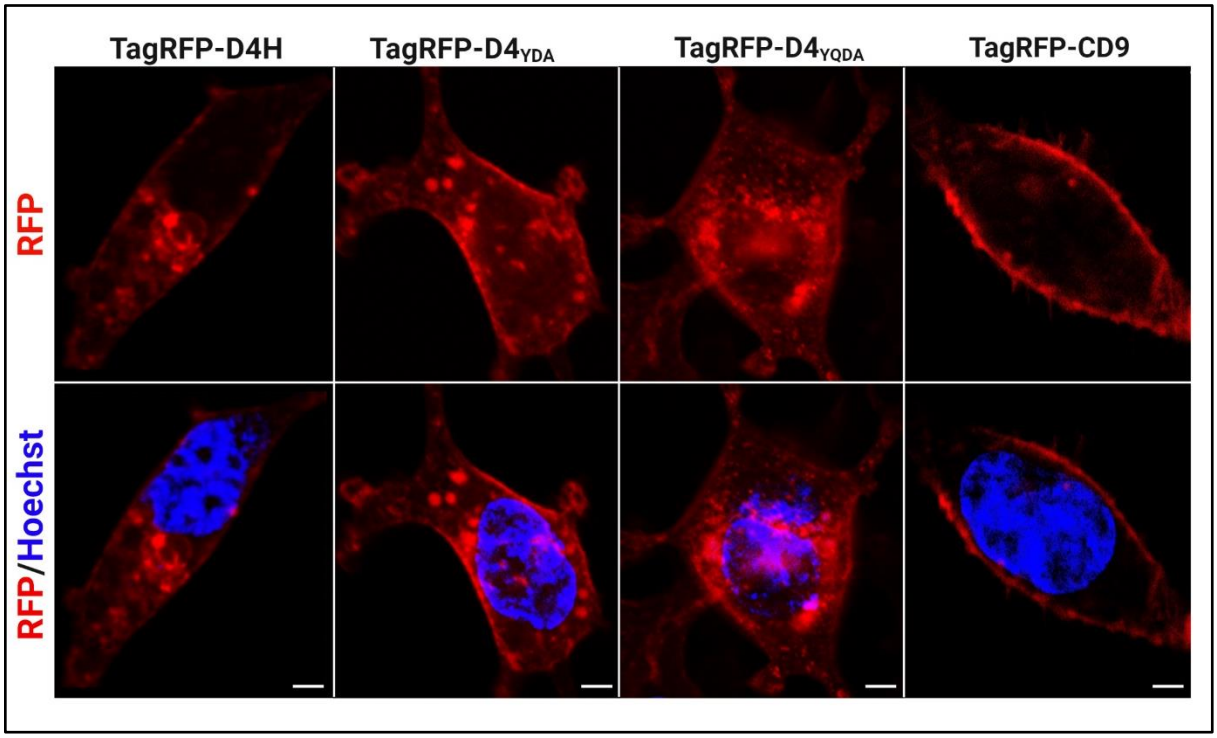

Fig 1.2.3: Intracellular expression of TagRFP-D4 and mutants compared with TagRFP-CD9. TagRFP-D4H, TagRFP-D4$_{YDA}$, TagRFP-D4$_{YQDA}$, and TagRFP-CD9 were stably expressed in HEK-293T cells, and their localization was analysed by live cell imaging. Red, TagRFP; blue, DAPI. Bar, 5 µm

1.2.4 Absolute fluorescence intensity of TagRFP enriched EVs in CM

To determine the enrichment of RFP in isolated EVs, CM were isolated from HEK-293T cells expressing each of the constructs as stated in (Fig. 1.2.2A) and RFP-enriched EVs were evaluated in derived CM by fluorescence spectrophotometer (Fig. 1.2.4A). As the absolute fluorescence intensity depicts an estimate of RFP-enriched EVs in CM, we found no statistically significant difference between fluorescence intensities of TagD4H and RFP-D4$_{YDA}$, while that of RFP-D4$_{YQDA}$, which has been reported to have the highest affinity to cholesterol was unexpectedly lower. As expected, the fluorescence value in CD9-EVs was higher than others which may be due to the RFP attachment to CD9's surface and captured by the spectrophotometer (Fig. 1.2.4B). Overall, these results suggests that RFPs can be loaded into D4-EVs and the fluorescence intensity of POI labelled with fluorescent protein can be detected in the cell's derived CM after EVs are secreted and isolated.

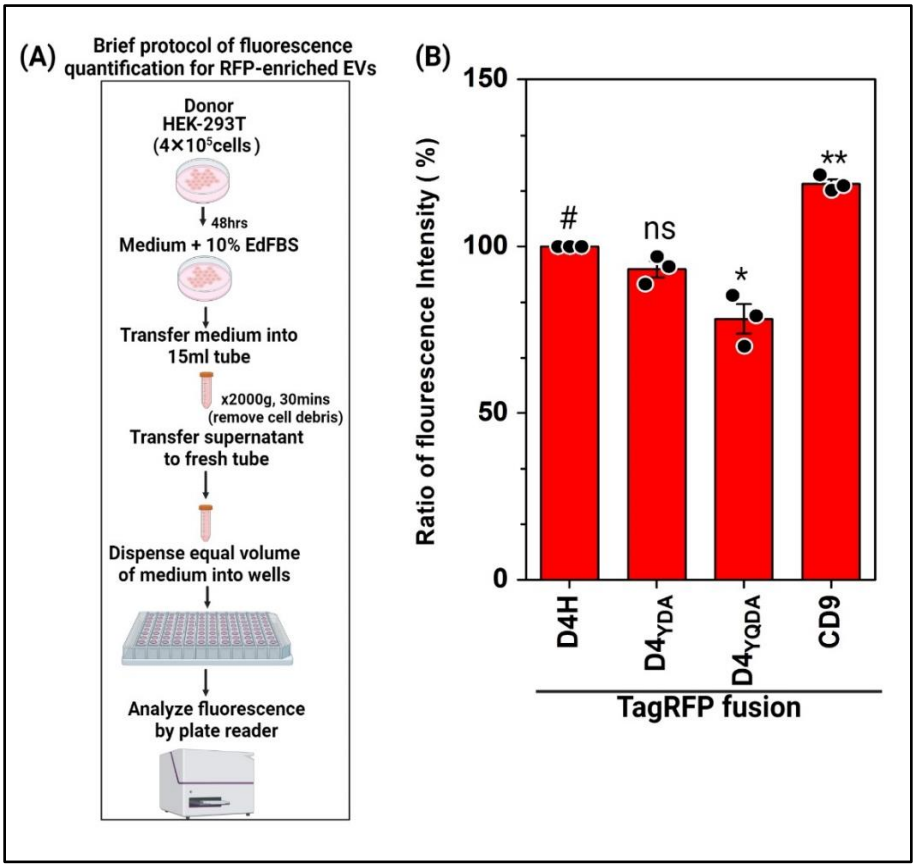

Fig 1.2.4: Fluorescence quantification of TagRFP loaded EVs in CM. (A) Brief protocol of fluorescence quantification of RFP-enriched EVs by spectrophotometer. (B) Quantification of fluorescent intensity of TagRFP in CM. The fluorescence intensity was normalized by cell number. The results of each group were shown as relative to the RFP-D4H (#). Graph shows three independent measurements with mean ± SEM. *$P < 0.05$, **$P < 0.005$ and n.s, not significant

1.2.5 Effect of cholesterol depletion on D4-mutant protein expression

To evaluate whether cholesterol depletion affects D4 protein expression and EV-loading efficiency, we performed Methyl-β-cyclodextrin (MβCD)-mediated cholesterol depletion and confirmed the reduction of the total protein levels of TagRFP-D4 variants, particularly in the case of TagRFP-D4$_{YQDA}$ (Fig 1.2.5). Although we could not assess the EV-loading efficiency due to the significant toxicity of this treatment.

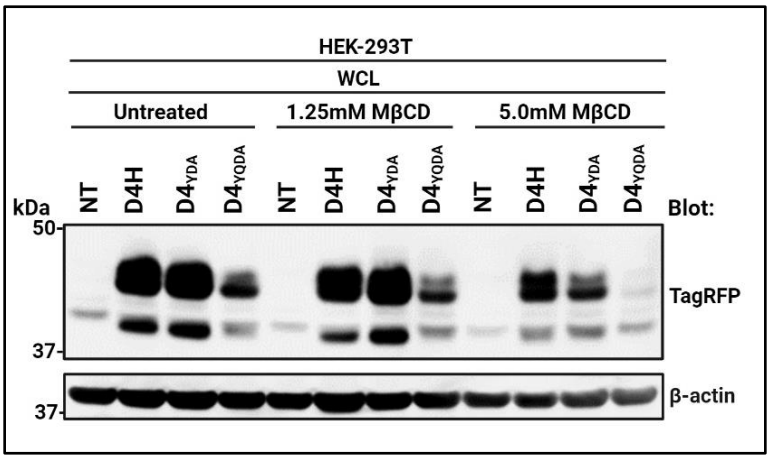

Fig. 1.2.5: Cholesterol levels affect total protein levels of TagRFP-D4 variants.
Cell lysates of HEK-293T cells stably expressing TagRFP-D4 variants treated with MβCD were subjected to immunoblotting with the indicated antibodies.

1.2.6 Expression efficiency of D4-mutants in MDA-MB-231 cells

To ascertain if protein expression is dependent on intracellular cholesterol levels, we first determined the efficiency of cholesterol measurement by Filipin III staining in HEK-293T cells at several concentrations (Fig 1.2.6A). Next, we compared cholesterol staining in stable cells expressing TagRFP-D4$_{YDA}$ constructs (Fig 1.2.6B). Furthermore, we characterized the D4 variants in MDA-MB-231 cells, which have relatively lower cholesterol levels compared HEK-293T cells (Fig 1.2.6B). Interestingly, in MDA-MB-231 cells, TagRFP-D4$_{YDA}$ and TagRFP-D4$_{YQDA}$ tended to show higher EV-loading efficiency compared to TagRFP-D4H.

However, the total protein level of TagRFP-D4$_{YQDA}$ was clearly lower than the other two (Fig 1.2.6C). These findings suggest that the EV-loading capacity and protein stability of D4 variants are influenced to some extent by intracellular cholesterol levels.

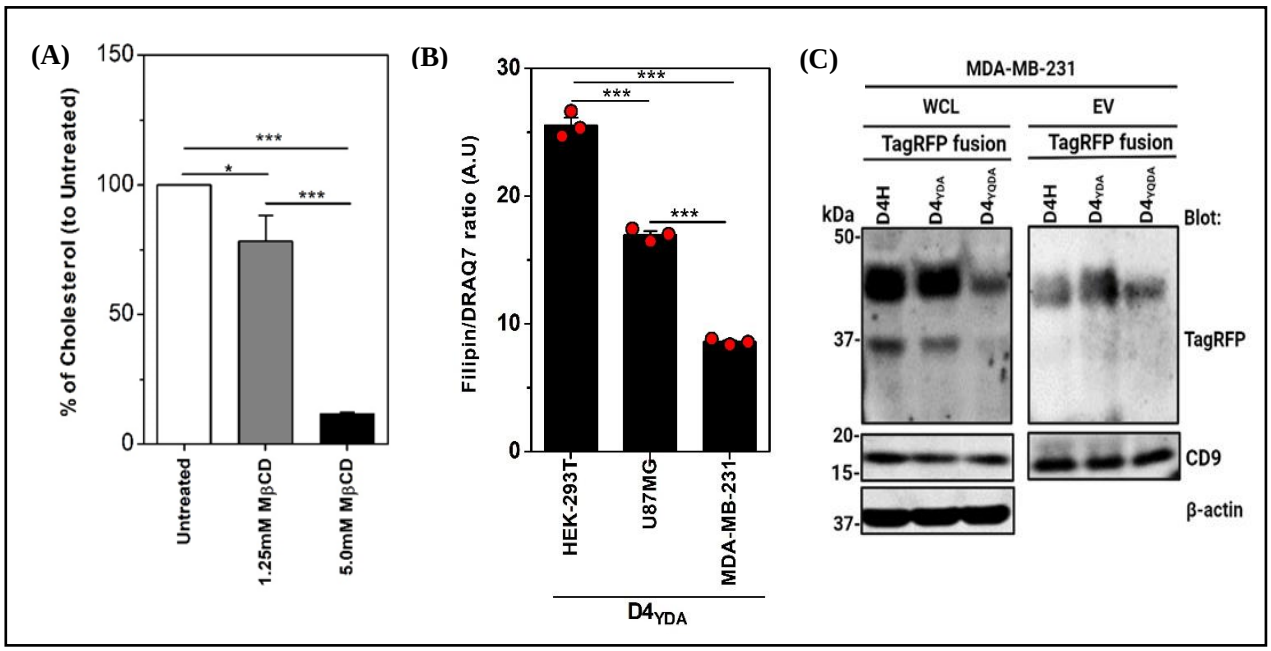

Fig. 1.2.6: Measurement of cholesterol levels based on Filipin III staining and D4-mediated EV-loading in MDA-MB-231 cells.
(A) HEK-293T cells were treated with MβCD at the indicated concentrations. Cells were stained with Filipin III and the fluorescence was normalized by cell count based on DRAQ7 staining. (B) HEK-293T, U87MG and MDA-MB-231 cells were stained with Filipin III and the fluorescence was normalized by cell count based on DRAQ7 staining. (C) Cell lysates and EV fractions of MDA-MB-231 cells stably expressing TagRFP-D4 variants were subjected to immunoblotting with the indicated antibodies.

1.2.7 Immunocapture of D4-EVs by CD9-positive EVs

To validate the interaction of D4$_{YDA}$-EV population with the highly enriched CD9 membrane protein, we isolated EVs from HEK293T cells expressing TagRFP tagged to either D4$_{YDA}$ or CD9 and captured D4$_{YDA}$ associated EVs using streptavidin magnetic beads slurry mixed CD9 biotinylated antibody. The expression level of RFP was evaluated by western blotting. The result showed that TagRFP- D4$_{YDA}$ EVs was successfully captured and detected in CD9-positive EVs which is considered as ectosomes (Fig 1.2.7) indicating the universality of

$D4_{YDA}$ as a potential tool for transporting POI into EVs including MVB-derived and PM-derived EVs.

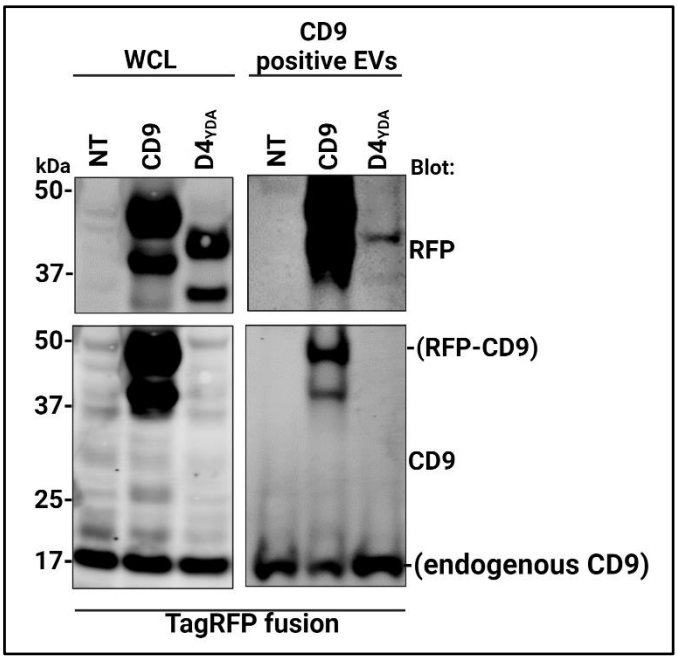

Fig 1.2.7: Western blot analysis of D4-EVs captured by CD9-based magnetic beads. CD9-positive EV was isolated using a biotin-conjugated CD9 monoclonal antibody and streptavidin magnetic beads. Presence of TagRFP-$D4_{YDA}$ in the EV fraction was analysed by western blot.

1.2.8 Evaluation of D4-bound EVs by Size Exclusion Chromatography

To further determine the characterization of D4-EVs, we confirmed that TagRFP-$D4_{YDA}$ was primarily found in EV-rich fractions separated by size exclusion chromatography (SEC). Distribution of TagRFP-$D4_{YDA}$ over the SEC fractions was slightly different from that of CD9, with TagRFP-$D4_{YDA}$ relatively concentrated in the earlier fractions compared to CD9 (Fig 1.2.8). The different distribution patterns of $D4_{YDA}$ and CD9 in the SEC fractions are consistent with previously mentioned results. Altogether, these data collectively suggest that $D4_{YDA}$ could be a valuable tool for transporting POIs into EVs.

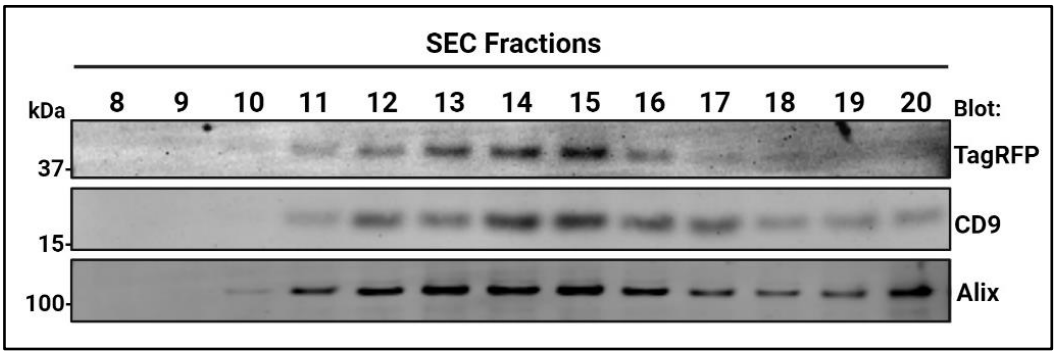

Fig 1.2.8. SEC fractions of CM from TagRFP-D4$_{YDA}$ expressing cells.
CM of HEK-293T cells stably expressing TagRFP-D4$_{YDA}$ was separated by SEC. EV-rich and EV-poor fractions were subjected to immunoblotting with the indicated antibodies.

1.3 Discussion

1.3.1 Model of POI

In this section, we report the capacity of domain four (D4) of PFO anchored on cholesterol-specificity to recruiting exogenous cargos into EVs. The basic steps for EV cargo recruitment often relies on the model or choice of cargo (*also known as POI)*, machinery for EV biogenesis and the biological technique for loading engineered cargos (*this is further elaborated in 2.0*). In this section, we choose TagRFP as a model of POI. TagRFP which has been previously reported as a monomeric red fluorescent protein (RFP) is characterized by high cellular brightness, complete chromophore maturation, high pH-stability and an extended fluorescence lifetime compared to its ancestors (Merzlyak et al., 2007; Shaner et al., 2008). While several homologs of *Aequorea victoria* green fluorescent proteins (avGFP) have been cloned from marine organisms in the last decade, majority of the fluorescent proteins (FP) that have been utilized for EV-studies are often in the green parts of the spectrum. In 2018 Kulichova et al., establish HeLa cell lines as a donor cell for secreting exosomes expressing TagRFP fused to CD63, and their western blot analysis shows that TagRFP can be detected in fractions of isolated EVs (Kulichkova, Selenina, Tomilin, & Tsimokha, 2018). Our results also shows that TagRFP can be loaded into EV fractions and detected by immunoblotting using RFP-based antibody. Moreover, intracellular localization of TagRFP tethered to D4-series and CD9 can be visualized with confocal microscopy. Although some degradation of TagRFP were detected in the lysate fractions of cells

expressing TagRFP construct, and this may have been due to TagRFP residual tendency to dimerize (Cranfill et al., 2016). Future studies are required to ascertain the effective and optimum fusion tags needed for characterization of EVs.

1.3.2 Machinery for EV loading

Previous studies have shown that the machineries that regulate the biogenesis of EVs includes the endosomal sorting complex required for transport (ESCRT) machinery (Colombo et al., 2013), the cytoskeleton (Thom et al., 2017), syndecan-syntenin-Alix pathway (Baietti et al., 2012), arrestin domain-containing protein 1 (ARRDC1) (Anand et al., 2018), tetraspanins (van Niel et al., 2011) and lipids (Trajkovic, 2008). A recent study showed that proteins containing amino acids sequences biochemically related to the KFERQ motif are loaded into exosomes through the lysosome-associated membrane protein 2, isoform A (LAMP2A) (Ferreira et al., 2022). Meanwhile, Strezenbach et al., demonstrated that by labelling a target protein, Cre recombinase with a WW tag leads to recognition by the L-domain containing protein Ndfip1 and thus, loaded into exosomes (Sterzenbach et al., 2017). On the other hand, tetraspanins have gained prominence in the recent times as markers of EVs that can be deployed for EV-engineering purposes due to their increased accumulation in EVs, and access to labelling since they are localized as membranous structures. Silva et al., loaded high levels of green fluorescent proteins (GFP) into EVs through tetraspanins CD9, CD63 and CD81 (Silva et al., 2021). Toribio et al., developed a quantitative method to evaluate EV uptake in recipient cells by engineering EVs to express EGFP-Renilla-split-tag fused tethered either CD9 or CD63 (Toribio et al., 2019). Similarly, several researchers have also incorporated luminescence reporters such as NanoLuc into EVs through several tetraspanins members (Kojima et al., 2018; Somiya & Kuroda, 2021a, 2021b). Not until recently did some studies show that tetraspanins engineered EVs may have specific limitations in the areas of precise cell targeting and in contribution to viral infectivity (Böker et al., 2018). Considering these limitations, we sought to utilize D4 as a cargo recruitment tool of POIs into EVs.

The roles that lipids and cholesterol plays in the biogenesis of EVs have not been fully understood, although it is proposed that the formation of intraluminal vesicles (ILV) - an

event that occurs in the endocytic channel leading to the generation of MVBs requires the lateral segregation of cargo within the limiting membrane of an endosome (Pfrieger & Vitale, 2018). This could also suggest that '*some components*' in inner leaflets of PM may account for EV biogenesis. Interestingly, cholesterol-rich microdomains are domiciled in EV membranes (Maxfield & van Meer, 2010). Also, D4 have been characterized as a water-soluble protein that binds to cholesterol sites within PM (Johnson & Heuck, 2014). Likewise, EVs (exosomes) have been reported to be highly enriched in cholesterol, glycosphingolipids, phosphatidylcholine, and sphingomyelin suggestive of the presence of lipid-rafts within them (Llorente et al., 2013). We therefore reasoned that, cholesterol in EV may serve as the putative sites for binding to D4, thus making D4 as a machinery for transporting foreign cargo into EV during its biogenesis.

Although the degree of cholesterol enrichment varies on the cell of origin and subpopulation of EVs. Our study shows that U87MG glioblastoma cells which have been reported to possess high levels of cholesterol content shows a slight elevation of TagRFP-D4H in EV fractions compared to other cell lines (Fig. 1.2.1 E) and we also confirmed that TagRFP can be incorporated into EVs through D4 in several cell lines confirming its versatility for EV-engineering purposes. Additionally, we examined the effects of methyl-β-cyclodextrin (MβCD)-mediated cholesterol depletion (Fig. 1.2.5). We found that 1.25 mM and 5.0 mM MβCD depleted cholesterol levels by approximately 20% and 90% (Fig. 1.2.6A), which were estimated based on Filipin III staining. However, we were not able to examine the effect of the cholesterol depletion on the EV-loading capacity of D4 variants, since this treatment induced significant cell death after the additional 48 h incubation in the EV-depleted medium, which is required for harvesting enough amounts of EVs and is very stressful for the cells by itself. On the other hand, by the time a clear reduction in cholesterol level was observed, the total protein levels of D4 variants were also clearly reduced, indicating that their stability are in fact affected by cholesterol levels (Fig. 1.2.5). In addition, we examined EV loading efficiency of D4 variants in MDA-MB-231 cells, which have relatively lower cholesterol levels compared to HEK-293T cells (Fig. 1.2.6B). $D4_{YDA}$ and $D4_{YQDA}$ showed higher EV-

loading efficiency than D4H (Fig 1.2.6C), indicating that higher affinity to cholesterol is more suitable for the EV-loading in the cells with lower cholesterol levels.

1.3.3 Enhancement of D4-affinity to cholesterol and loading into EV

D4 of PFO binds specifically to cholesterol rich membranes with high affinity but not with other membrane molecules (Ohno-Iwashita, Iwamoto, Ando, & Iwashita, 1992), however, this binding also requires cholesterol concentration to exceed a certain threshold (Heuck, Hotze, Tweten, & Johnson, 2000). By identifying mutations in PFO such as Cys459Ala, the threshold required for binding can be considerably altered (Moe & Heuck, 2010). Site-directed mutagenesis is often employed in protein engineering and plasmid construction to change primary DNA sequences such as base substitutions and base additions or deletions for the purpose of studying changes in protein response after mutation conferment (Kunkel, 1985; Zeng et al., 2018). Through the introduction of mutations to PFO yielding several PFO derivatives, the binding affinity of PFO to cholesterol can be controlled (Johnson et al., 2012). By introducing point mutation to D4 which led to an enhanced affinity to cholesterol, the localization of D4 to PM was improved (Maekawa & Fairn, 2015). In our study we also confirmed mutations that are known to increase affinity to cholesterol clearly shows distinct localization to PM and vesicular structures in cytoplasm. Moreover, these D4-mutants are also accumulated in EV fractions. In contrast, our data also shows that increased affinity of D4 to cholesterol does not translate to high efficiency in cargo loading. These may occur because additional mutations may lead to biochemical changes in lipid-raft domain of EVs where cholesterol is enriched, thus altering the encapsulation behaviour of EVs during its biogenesis. Also, we confirmed that EV derived from D4-mutant can be detected by CD9-positive EVs (Fig 1.2.7). Though we did not ascertain if all D4-EVs share similar interaction with CD9-EVs, further studies are needed to examine the effects of several mutations to D4 on EV functionality. Conclusively, we were able to detect the isolation of TagRFP-D4$_{YDA}$ EV by SEC in EV-rich fractions than non-EV fractions suggesting that D4-bound cargo is indeed loaded into EVs (Fig 1.2.8).

Experimental Finding 2.

Efficiency of protein loading and vesicle internalization between D4-EVs and CD9-EVs.

2.0 Brief Introduction

The EV encapsulation of exogenous POIs is a highly essential process of ensuring its effectiveness as a delivery vehicle. The stability of encapsulated POIs in EVs and its functionality after delivery by EV in recipient cells are challenges that still require further elucidation. Several methods have been developed to load exogenous cargos into EVs and they are mainly classified into 1) pre-loading and 2) post-loading (Chen et al., 2021; Fuhrmann, Serio, Mazo, Nair, & Stevens, 2015; Peng et al., 2020). In the pre-loading process, parental cells are transfected with plasmids encoding engineered DNA or by using liposome-based transfection to incorporate foreign genetic small molecules into EVs. The parental cells are then cultured into donor cells for isolating EV packed with engineered cargos. It is important to mention that this approach is only limited to EVs derived from cell-culture and may not be applied to EV derived from other sources such as plasma, saliva, and similar fluids (KW & Kierulf, 2015). In the post-loading process, EVs are isolated and purified from selected sources and then passively or actively stimulated for exogenous incorporation of POIs using techniques such as electroporation, free-thaw cycles, ultrasound-induced sonication, click chemistry and direct co-incubation by mixing (Fu, Wang, Xia, & Zheng, 2020b; Mehryab et al., 2020). The disruption of EV membrane integrity, inefficient cargo loading capacity, aggregation of vesicles, toxicity and increase in haemolytic activity are some of the challenges of the post-loading process (Peng et al., 2020). In this report, we used the pre-loading approach to incorporate several variants of red fluorescent proteins into EV by stably transfecting parental cells with selected plasmids. We isolated purified EVs from donor cells and compared the efficiency of loading and uptake between D4 and another widely used member of the tetraspanin family (CD9).

In experimental finding 1, we utilized TagRFP as a model of POI for recruitment into EVs. However, RFP have been reported to suffer from low ensemble brightness, slow maturation time and may be degraded due to severe residual dimerization in mammalian cells

(Wiedenmann, Oswald, & Nienhaus, 2009). To improve on the bioimaging of D4-EVs in recipient cells, we tested brighter variants of RFP, FusionRed MQV (FR-MQV) (Jimenez et al., 2020) which is a derivative of TagRFP, and mScarlet-I (Gadella et al., 2023; S. Wang, Ding, Xue, Hou, & Sun, 2018). While FR-MQV exhibits a fluorescence lifetime of 2.8 ns and significantly improved *in vitro* brightness, mScarlet-I has a fluorescence lifetime of 3.9 ns, a fast chromophore maturation, higher intracellular brightness, and low cytotoxicity (Bindels et al., 2016). We therefore selected mScarlet-I as a model of POI for further analysis in this section.

The routes and mechanisms of EV uptake in recipient cells (Fig 2.0.1) have been reported to occur through these pathways, 1) Clathrin-mediated endocytosis, 2) Lipid-raft mediated endocytosis, 3) Caveolin-mediated endocytosis, 4) Phagocytosis and 5) Micropinocytosis (Gurung, Perocheau, Touramanidou, & Baruteau, 2021).

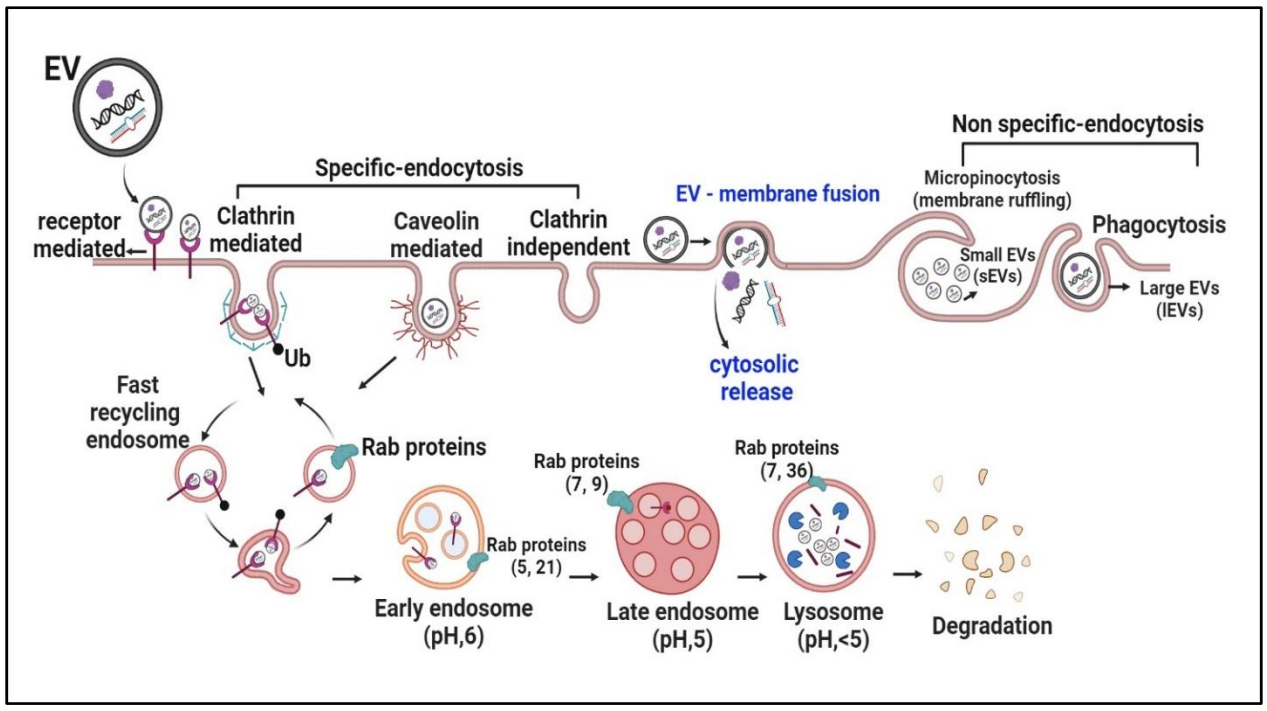

Fig 2.0.1: Routes and mechanisms of EV uptake in recipient cells.

While there have been reports suggesting the possible fusion of EVs to recipient's cells membrane, the experimental evidence to support this remains controversial (Mulcahy, Pink, & Carter, 2014; Parolini et al., 2009; Somiya, 2020). The uptake efficiency of EVs is also

reported to be dependent on the level of endocytosis-related molecule expression in recipient cells such as caveolin-1 (Horibe, Tanahashi, Kawauchi, Murakami, & Rikitake, 2018), this further suggests that EV maybe selectively incorporated into recipient cells according to their physiological state. Parolini et al, showed that the microenvironmental pH on recipient cells is a key factor for enhancing EV entry specifically into tumour cells (Parolini et al., 2009). On the other hand, endogenously produced and engineered EVs have also been reported to play crucial roles in the uptake process based on the EV cells of origin, heterogeneity, and cargo composition (K. O'Brien, Ughetto, Mahjoum, Nair, & Breakefield, 2022). Moreover, several techniques have been developed for evaluating or quantifying EV uptake such as using fluorescence or luminescence reporter proteins tagged to EV proteins for tracking the biogenesis, uptake, and cargo release of EVs. Previously, Gupta et al., used several luciferase enzymes tethered to tetraspanins CD9, CD63 and CD81 for achieving real-time in-vitro and in-vivo imaging of EV internalization (Gupta et al., 2020).

While there are have been numerous studies on the uptake mechanisms of tetraspanins EVs, **the uptake capability of D4-EVs remains unknown**. Therefore, in this section, we evaluated the uptake efficiency of D4-EVs in MDA-MB-231 cells using immunoblotting, fluorescence quantification and confocal imaging. We also tested if uptake of D4-EVs is analogous to that of the widely used CD9-EVs.

2.1 Materials and Methods

2.1.1 Plasmids

Plasmids were constructed as described in *1.1.1*.

2.1.2 Preparation of EVs for uptake assay

EVs were isolated from donor cells (7×10^5) as previously described in *1.1.3*. After precipitation, EVs from 5ml of donor cell supernatant were concentrated to 100ul of EVs in 1XPBS and protein concentration was determined. To determine the purity of EVs before cell treatment, the absence of GM130 protein was detected in EV fractions by immunoblotting. Recipient cells were thereafter treated with 20µg of total EV proteins for 12-24hr for evaluating uptake efficiency.

2.1.3 Immunoblotting of recipient cells treated with D4-EVs

To confirm that residues of EV treated to recipient cells are not roughly attached to cell's surface, cells were washed thoroughly with 1XPBS (thrice) and immunoblotting was performed as previously described in *1.1.5.* Detected levels of internalized mScarlet-I EVs were probed with a polyclonal mCherry antibody.

2.1.4 Fluorescence quantification of internalized D4-EVs

For quantification of cellular uptake by plate reader, 1 ×10^4 cells MDA-MB-231 cells were seeded into 96-well plates and cells were treated with EVs in CM or PEG-EVs. 12 h after incubation, culture medium was aspirated, and cells were washed with PBS thrice and replaced with phenol red free media. Fluorescence signal was measured by plate reader in a bottom-optic mode with equal RFP settings for all culture plates (Ex 540-20 nm, Em = 590-20 nm with an autofocus = 565 nm and gain = 1500).

2.1.5 Live cell fluorescence microscopy of internalized D4-EVs

To evaluate the uptake efficiency of mScarlet-I derived $D4_{YDA}$ or CD9 EVs by live imaging, MDA-MB-231 cells were seeded into a glass bottom dish. After incubation with EVs for 12 h, the medium was aspirated, and the cells were washed thrice with PBS and then replaced with fresh medium containing 2.5 µg/ml of Hoechst 33342 (nuclei) and then stained with 0.5mg/ml of Calcein-AM (cytosol). Fluorescence images of live cells were visualized with Leica TCS SP8 confocal laser scanning microscope (Leica Microsystems), installed with a heater and CO2 incubator.

2.2 Results

2.2.1 Cellular localization and fluorescence quantification of three RFP tags fused to $D4_{YDA}$

The creation of fluorescent proteins (FP) has transformed the field of biological imaging, however the utility of most FP in mammalian cells is restricted by its relatively subdued fluorescence brightness (Tsien, 1998). The cellular brightness of FPs greatly relies on its molecular brightness, which is determined by the product of the molar extinction coefficient and the fluorescence quantum yield (Cranfill et al., 2016). Several FPs with higher quantum

yield have been reported till date (Goedhart et al., 2012; Lambert, 2019; Sarkisyan et al., 2015). To therefore improve on the bioimaging of D4-EVs in recipient cells, we tested brighter variants of RFPs, FusionRedMQV (FR-MQV) (Jimenez et al., 2020), which is a derivative of TagRFP, and mScarlet-I which is brightest so far observed (Bindels et al., 2016; Gadella et al., 2023). Our study shows that MDA-MB-231 cells stably expressing individual the constructs were imaged by confocal microscopy to capture cellular brightness and reveals that m-Scarlet-I-D4$_{YDA}$ cells were much brighter than others (Fig 2.2.1A). Moreover, the intracellular localization of D4$_{YDA}$ was similar amongst the three FPs. Additionally, the cellular fluorescence quantification showed that mScarlet-I cells were significantly higher than TagRFP and FRMQV cells (Fig 2.2.1B). Since EVs share similar properties with their cells of origin (Kalluri & LeBleu, 2020), we believe EVs derived from mScarlet-I donor cells will exhibit higher fluorescence in medium when compared to others and ultimately increasing their chance of detection or visualization after internalization in recipient cells. Confirming this point, we harvested CM from MDA-MB-231 cells expressing these constructs, measured fluorescence in each of the CM, and compared to control cells. Fluorescence was increased in CM of cells bearing mScarlet-I-D4$_{YDA}$ up to 4 folds and 2 folds when compared with TagRFP-D4$_{YDA}$ and FR-MQV-D4$_{YDA}$, respectively (Fig 2.2.1C), indicating that mScarlet-I enhances fluorescence detection when used to label EVs by D4$_{YDA}$. We therefore choose m-Scarlet-I as a model of POI for further analysis.

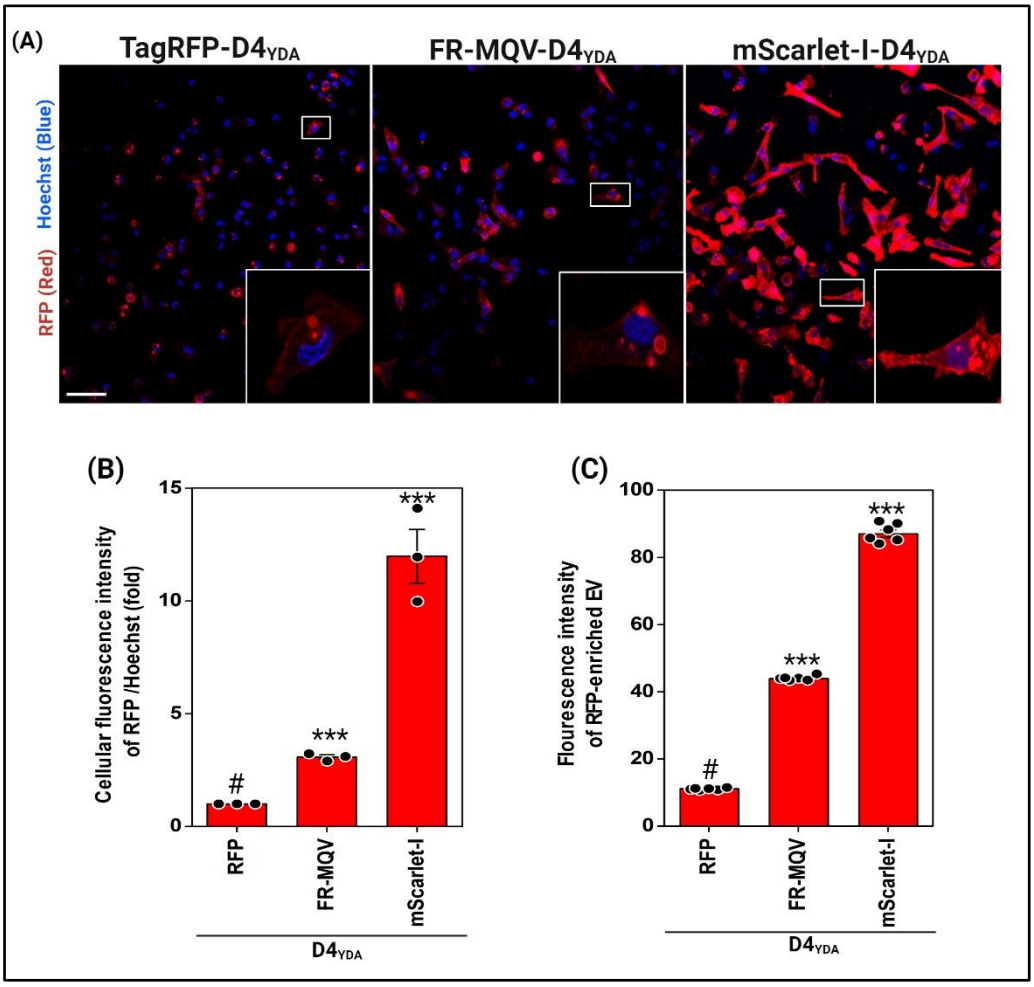

Fig 2.2.1: Comparison of fluorescence intensities between three fusion-tags. (A) TagRFP-D4$_{YDA}$, FR-MQV-D4$_{YDA}$ and mScarlet-I-D4$_{YDA}$ were stable expressed in MDA-MB-231 cells and their cellular brightness was captured by live-cell-imaging. Bar; 75μm. (B) Quantification of cellular fluorescent intensity in MDA-MB-231 cells stably expressing 3 different RFPs by spectrophotometer. The fluorescence intensity was normalized by viable cells stained with Hoechst 33342. Graph shows three independent measurements with mean ± SEM. ***$P < 0.0001$. (C) Quantification of fluorescent intensity of RFP-enriched EVs from MDA-MB-231 cells stably expressing 3 different RFPs. The fluorescence intensity was normalized by cell number. Graph shows six independent measurements with mean ± SEM. ***$P < 0.0001$.

2.2.2 Analysis of stable MDA-MB-231 donor cells expressing mScarlet-I POIs

To confirm the loading efficiency of mScarlet-I into EVs, MDA-MB-231 donor cells expressing mScarlet-I-D4$_{YDA}$ were prepared for EV isolation (Fig 2.2.2A). Western blot analysis of EV fraction and the total lysates from the donor cells, using an mScarlet-I-reactive antibody, suggested that mScarlet-I was loaded into EV fractions by D4$_{YDA}$ (Fig 2.2.2B), with the analogous efficiency as CD9 (Fig 2.2.2C) as determined by densitometry analysis.

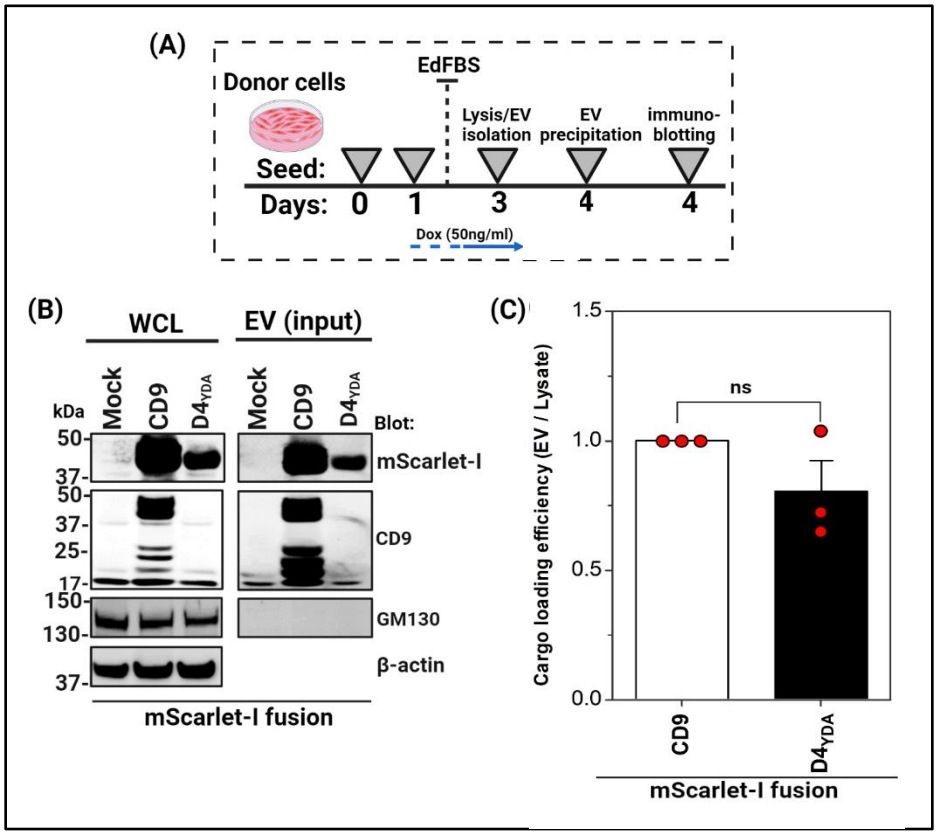

Fig 2.2.2: Comparison in loading efficiency between D4$_{YDA}$-EVs and CD9-EVs. (A) Experimental set-up for EV isolation from stable MDA-MB-231 c ells. (B) The mScarlet-I-D4$_{YDA}$ and mScarlet-I-CD9 were stably expressed in MDA-MB-231 cells. Cell lysates and EV fractions were analysed by western blot using indicated antibodies. mScarlet-I was detected by an mCherry antibody. (C) Quantification of western blots (n = 3) described in (B). The ratio of mScarlet-I in the EV fraction to lysate was plotted and normalized to CD9. The graph shows mean ± SEM from three different experiments. Values for NT samples were subtracted from those of CD9 and D4$_{YDA}$ samples. n.s, not significant (P = 0.2412).

2.2.3 Uptake analysis of internalized mScarlet-I EVs by confocal microscopy

We employed live-cell imaging to characterize EV exchange and uptake in MDA-MB-231 cells. Fluorescence images by confocal microscopy shows distinct uptake of $D4_{YDA}$-EVs in the cytosolic region of cells with possible localization to endosomal structures. Although we did not ascertain whether $D4_{YDA}$-EVs colocalizes with specific endosome makers such as Rab5 or Rab7, as a previous study indicates that GFP-CD63 derived EVs are localized within endosomal structures when probed with electron microscopy (Joshi, de Beer, Giepmans, & Zuhorn, 2020). The route of EV internalization has been widely reported to occur through endocytosis and onward transport into endosomes (Kalluri & LeBleu, 2020). Moreover, cytosolic staining of recipient cells with CalcienAM reveals that $D4_{YDA}$-EVs are actively functional within the region. Meanwhile, CD9-EVs were observed to be localized to the periphery of plasma membrane (*see white arrows*, Fig 2.2.3) as well as in huge vacuolar structures. This data further shows that substantial fractions of CD9-EVs are not internalized by cells and may be trapped on cell surface during the uptake process.

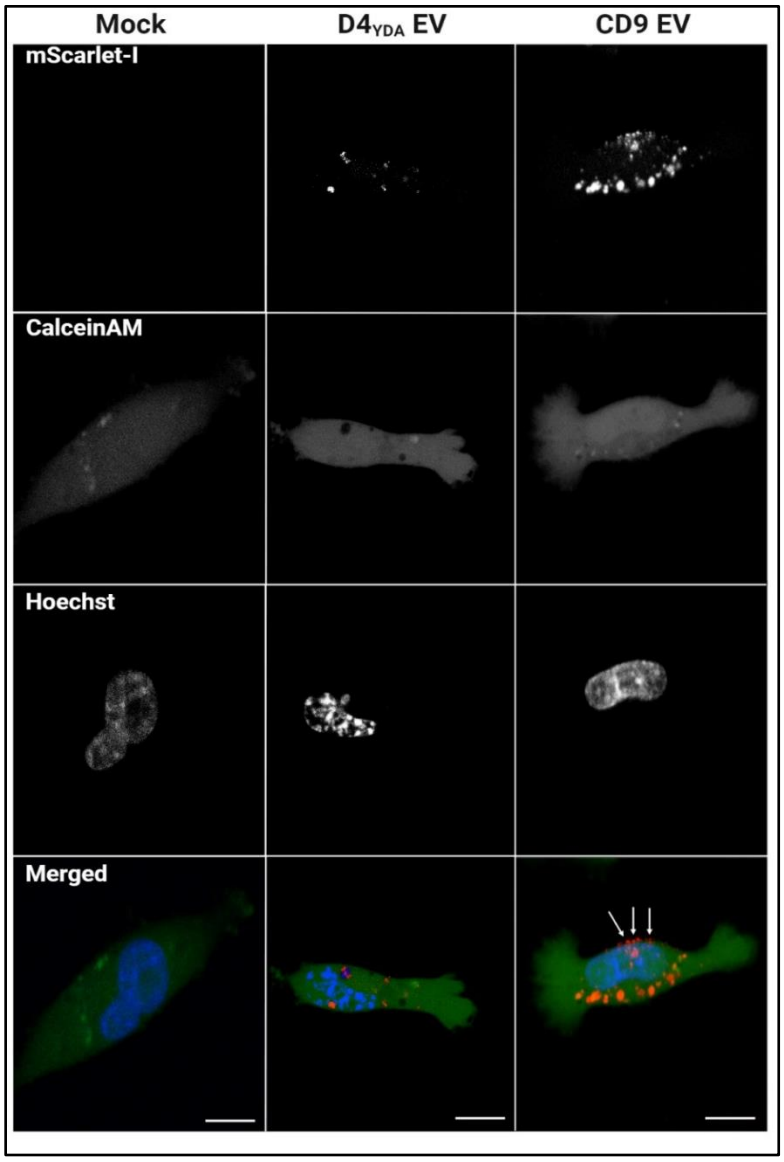

Fig 2.2.3: Live imaging of recipient cells uptake of $D4_{YDA}$-EVs and CD9-EVs. (A) Confocal microscopic images of EVs internalization and localization in recipient MDA-MB-231 cells. Cells were incubated with EVs containing mScarlet-I-$D4_{YDA}$ or mScarlet-I-CD9. Cytoplasm of the recipient cells were stained with CalcienAM. Arrows indicate EVs captured on the cell surface. Red, mScarlet-I; green, CalcienAM; blue, Hoechst 33342. Bar, 5 μm.

2.2.4 Comparison in uptake efficiency between D4-EVs and CD9-EVs.

To evaluate the uptake efficiencies between $D4_{YDA}$-EVs and CD9-EVs, we collected the EV fraction from donor cells expressing mScarlet-I-$D4_{YDA}$ or mScarlet-I-CD9 (Fig 2.2.4A), and then treated the EVs to recipient MDA-MB-231 cells for a period of 24hrs in a temperature dependent manner (Fig 2.2.4B). To distinguish between attachment (but not uptake) and uptake of EVs, we treated the recipient cells with EVs at 4°C (without uptake) or 37°C (with uptake). We confirmed that D4-EVs were clearly detected in the 37°C-treated cells while only marginally retained on the surface of 4°C-treated cells. Of note, quantification results suggest that when the amount of the cell surface-attached EVs are considered, D4-EVs show better uptake efficiency than CD9-EVs (Fig 2.2.4 D). This high uptake of CD9-EVs as captured by quantified may be rather due to EV-attachment to cell's surface rather than EV-internalization (Fig 2.2.4 C). CD9 mediated uptake of EVs have been previously reported especially as tetraspanins EV modulates selective targeting of recipient cells (Miki et al., 2018; Nigri et al., 2022). The cell line model used as recipient or acceptor cells have also contributed to the uptake process of CD9-EVs due to high association of β-1 integrins adhesion receptors with CD9 (H. X. Wang, Li, Sharma, Knoblich, & Hemler, 2011). In contrast, a recent study strongly opposes that CD9 present on recipient cells are not required for EV uptake and are in fact dispensable to mediate any form of membrane fusion with exogenous CD9-EVs (Tognoli et al., 2023). Some studies reports that anti-CD9 antibody inhibited EV-uptake within recipient cells suggesting the role that CD9 plays a role in EV-uptake (Nigri et al., 2022; Santos et al., 2019). All these discrepancies point to the fact that, despite the wide acceptance of CD9s for recruiting foreign cargos into EVs, their uptake ability remains disputable and questionable. These results further demonstrate that D4-EVs are indeed taken up by the recipient cells and showed a significant increase in cellular uptake when compared with CD9-EVs. Further studies are required to assess uptake of D4-EVs across multiple cell lines and to also test the effect of EV-inhibitors on the uptake of D4-EVs.

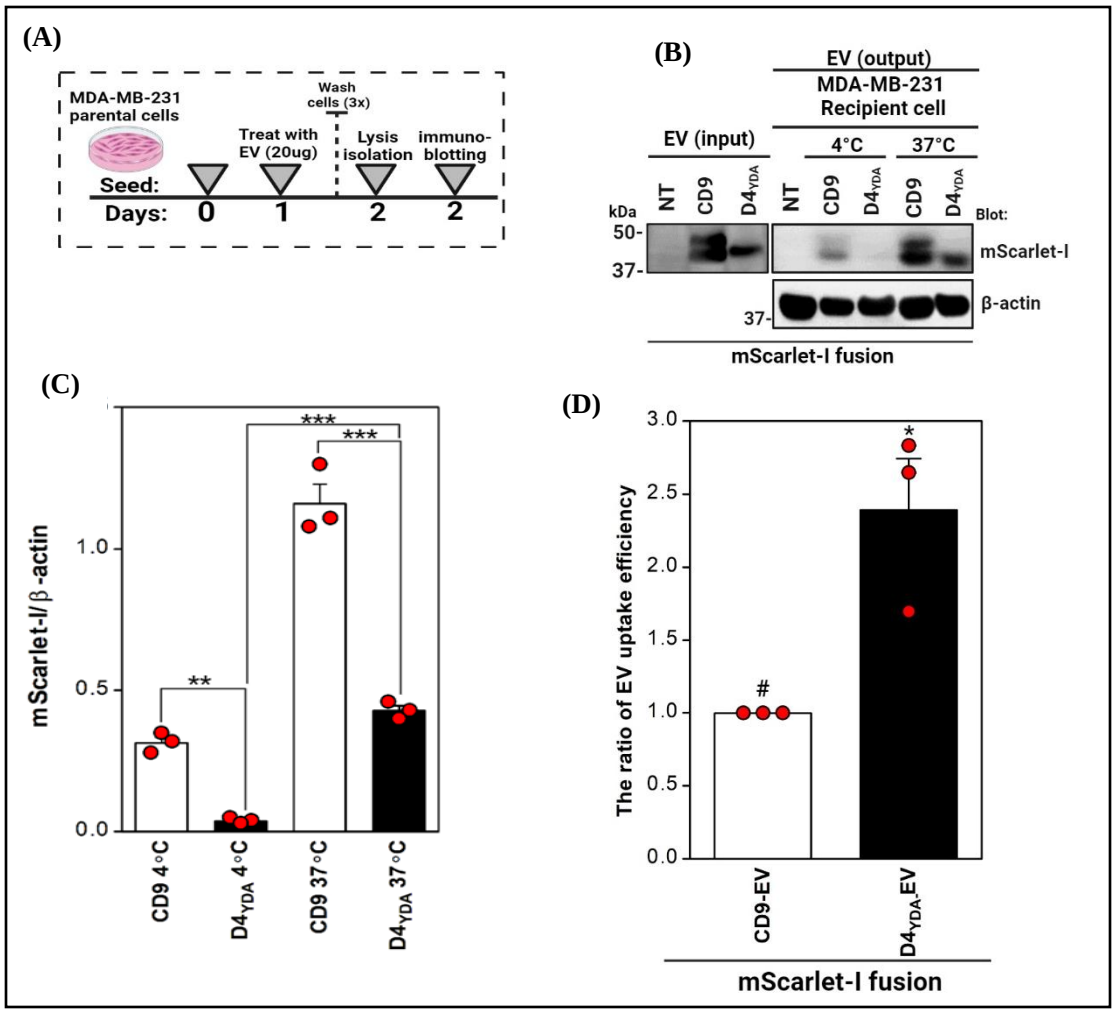

Fig 2.2.4: Comparison in uptake efficiency between D4$_{YDA}$-EVs and CD9-EVs. (A) Experimental set-up of EV treatment isolated from mScarlet-I-D4$_{YDA}$ or mScarlet-I-CD9 stably expressing cells. (B) EVs containing mScarlet-I-D4$_{YDA}$ or mScarlet-I-CD9 were isolated as indicated in (A), and 20 µg of total EVs were treated with recipient MDA-MB-231 cells for up to 24 h at 37°C (demonstrating EV uptake) and at 4°C (no EV uptake). EV uptake in the recipient cells were analysed by western blotting using indicated antibodies. (C) Quantification of western blot as described in (B). The total levels of mScarlet-I expression in EV fractions of both CD9-EVs and D4$_{YDA}$-EVs were plotted and normalized to Actin. Graph shows densitometry from three different experiments. Statistical analysis were performed by student t-test, ***P < 0.0001. (D) Quantification of EV uptake described in (B). The uptake efficiency was calculated as an average using the formula: [(37°C – NT) – (4°C – NT)] / (Input EV – NT), where each variable represents mScarlet-I normalized by β-actin. The graph shows mean ± SEM from three different experiments. The values of CD9 were set to 1.0 and the results are shown relative to CD9 (#). * $P < 0.0$

2.2.5 Colocalization of D4-EVs and CD9-EVs with endosomal proteins

To further validate the internalization of both D4 and CD9-EVs, we performed fluorescence microscopy to evaluate colocalization of EVs with several endosome proteins (Fig 2.2.5).

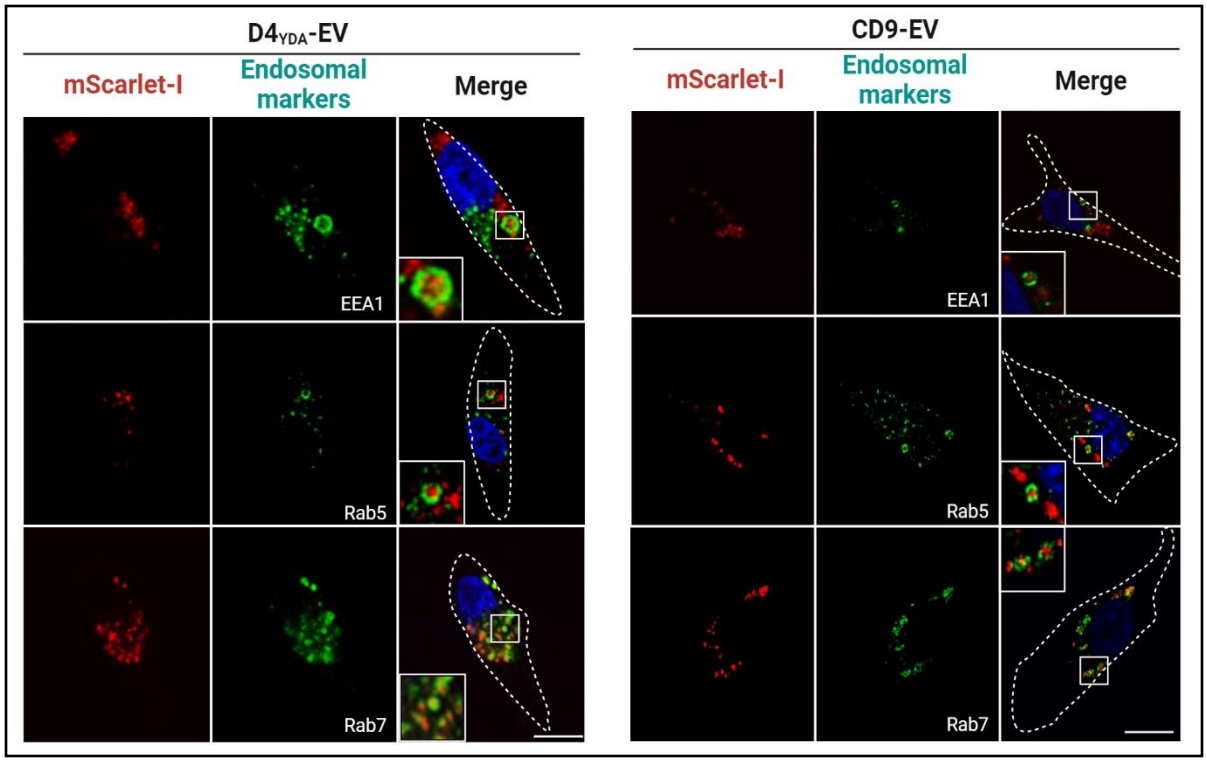

Fig 2.2.5: Colocalization of D4-EVs and CD9-EVs with endosomal proteins. Confocal microscopic images show EV internalization and localization in recipient MDA-MB-231 cells. Cells were incubated with EVs containing mScarlet-I-D4$_{YDA}$ or mScarlet-I-CD9, followed by staining of endosomal markers for early endosomes (EEA1 and Rab5) and late endosomes (Rab7). To visualize the cell periphery (dotted lines), α-tubulin was also immuno-stained. White squares indicate enlarged views. Red, mScarlet-I; green, endosomal markers; blue, DAPI. Bar, 5 μm.

2.3 Discussion

2.3.1 mScarlet-I: an effective fusion tag for characterization of EVs

In this section, we comparatively analysed the cargo loading efficiency between D4-EVs and CD9-EVs. mScarlet-I was incorporated into EVs as POIs and the protein expression was evaluated in the whole cell lysates and EV fractions. In fig 2.2.1, we confirm m-Scarlet-I intrinsic and intracellular brightness exceeds that of FR-MQV and TagRFP by confocal microscopy. The intrinsic brightness of mScarlet-I is because of the multiple rounds of site-directed mutagenesis applied to native RFP while screening for increased brightness and proper maturation to generate a high quantum yield of mScarlet variant with single amino acid substitution termed 'mScarlet-I' (Bindels et al., 2016). The absorption and emission maxima of mScarlet-I are 569nm and 594nm respectively, with a quantum yield of 0.70. mScarlet-I is considered as a versatile FP fusion tag for biological imaging. A recent study reported that mScarlet (anti-derivative of mScarlet-I) does not interfere with colocalization of CD63 targeting to lysosomes suggesting that mScarlet does not affect trafficking of endosome structures (Sung et al., 2020). We did not confirm if mScarlet-I exhibits similar colocalization properties as mScarlet, but our data shows vivid and enhanced localization of $D4_{YDA}$-mScarlet-I to plasma membrane and distinct vesicles in cytosol. Likewise, the isolated EVs in CM from $D4_{YDA}$-mScarlet-I showed an increase in florescence up to 62% and 39% when compared with $D4_{YDA}$-FR-MQV and $D4_{YDA}$-TagRFP respectively.

2.3.2 D4-EVs are analogous to CD9-EVs in cargo loading and uptake

Many studies have evaluated the enrichment levels of cargo proteins loaded into EVs, however the loading efficiency of POI by selected EV-sorting proteins have raised numerous concerns (Osteikoetxea et al., 2022). 12 candidates of EV-sorting proteins were screened for cargo loading ability using GFP as an intraluminal cargo and the results showed that vesicular loading of GFP is more efficient when tagged with membranous proteins (CD9, CD63 and MYR) as opposed to cytosolic proteins (Alix, Syndecan-1 and Lamp2b) (Corso et al., 2019). In our study, we selected a widely known EV membrane protein – CD9 and compared with

our developed candidate, D4, which is also anchored to cholesterol as a lipid-binding protein. Our results shows that cargo loading efficiency of D4 is analogous to that of CD9, suggesting that D4 is a viable candidate for loading exogenous cargo into EVs. Further studies are required to ascertain the versatility of D4 in loading a wide range of engineered cargos into EVs. We also evaluated the uptake efficiency of D4-EVs compared to CD9-EVs in recipient MDA-MB-231 cells and our results showed that the uptake efficiency of D4-EVs is much higher than that of CD9-EVs considering surface attachment by CD9-EVs. Furthermore, fluorescence images of recipient cells revealed co-localization of CD9-EVs and $D4_{YDA}$-EVs with endosomal markers EEA1, Rab5, and Rab7. These results demonstrate that $D4_{YDA}$-EVs are efficiently taken up by recipient cells, making them suitable for EV engineering and visualization.

Experimental Finding 3

Intracellular protein delivery of D4-EVs assisted by fusogenic VSV-G

3.0 Brief Introduction

EVs (specifically exosomes) are known be vehicles for intercellular communication by transferring protein and RNA molecules from donor cells to recipient cells (Skog et al., 2008). While EVs can be naturally taken up by cells through several endocytic channels as discussed in *2.0,* the direct delivery of EV cargo into cytosol of recipient cells have raised numerous debates in the EV field. Several researchers have since sought to develop experimental evidence explaining the 'EV cargo transfer hypothesis' (Albanese et al., 2021; Somiya, 2020; Somiya & Kuroda, 2021a). The cytosolic content release of EV cargo has been speculated to occur through the following mechanisms: 1) direct fusion with cellular plasma membrane, (Parolini et al., 2009; Valadi et al., 2007) 2) kiss and run fusion with endoplasmic reticulum (Heusermann et al., 2016), 3) fusion with endosomal membrane (Yao et al., 2018), and 4) endosomal rupture (Del Conde, Shrimpton, Thiagarajan, & López, 2005; Joshi et al., 2020; Mathieu, Martin-Jaular, Lavieu, & Théry, 2019). In contrast to EVs, viruses have been reported to deliver genetic materials into host cells by utilizing viral proteins that mediate specific receptor binding, membrane fusion and cellular uptake to deliver their cargo into host cells (Grove & Marsh, 2011; Moller-Tank, Kondratowicz, Davey, Rennert, & Maury, 2013). Since EVs and viruses share common transport mechanisms, attempts have been made by others to adopt the direct fusion by viruses as a model for EV cargo delivery (Somiya & Kuroda, 2022; van Dongen, Masoumi, Witwer, & Pegtel, 2016).

Recently, Somiya et al., reported the cytoplasmic delivery of EV cargos into recipient HEK-293T cells by utilizing FK506 binding protein fused to CD81 (Somiya & Kuroda, 2022) and evaluated cargo release with a split-luciferase system assisted with virus derived fusogenic proteins (Somiya & Kuroda, 2021a). Joshi et al, identified the intracellular sites for EV cargo release through an anti-GFP fluobody tagged to CD63 that specifically recognizes the EV cargo and demonstrated that cargo release occurs from endosomes/lysosomes (Joshi et al.,

2020). Albanese et al., also reported that EVs binds to the surface of recipient cells but do not deliver cargo into the cytosol of recipient cells except in the case of EVs engineered with ectopic fusogenic moiety such as VSV-G (Albanese et al., 2021). The commonalities between these studies and many more is the engineering of EVs with tetraspanin family proteins such as CD9, CD63 and CD81. Tetraspanins modulates cell-cell fusion and their overexpression in cells have been reported to affect precise cell targeting, enhance viral entry and trigger integrin activation as stated in *1.0.* While we have established the uptake capability of D4-EVs by recipient cells in the previous section, **it is unknown if D4-EVs also possess the capacity for protein delivery into recipient cells. We therefore propose a schematic model for the internalization and cargo release of D4-EVs (Fig 3.0.1)**

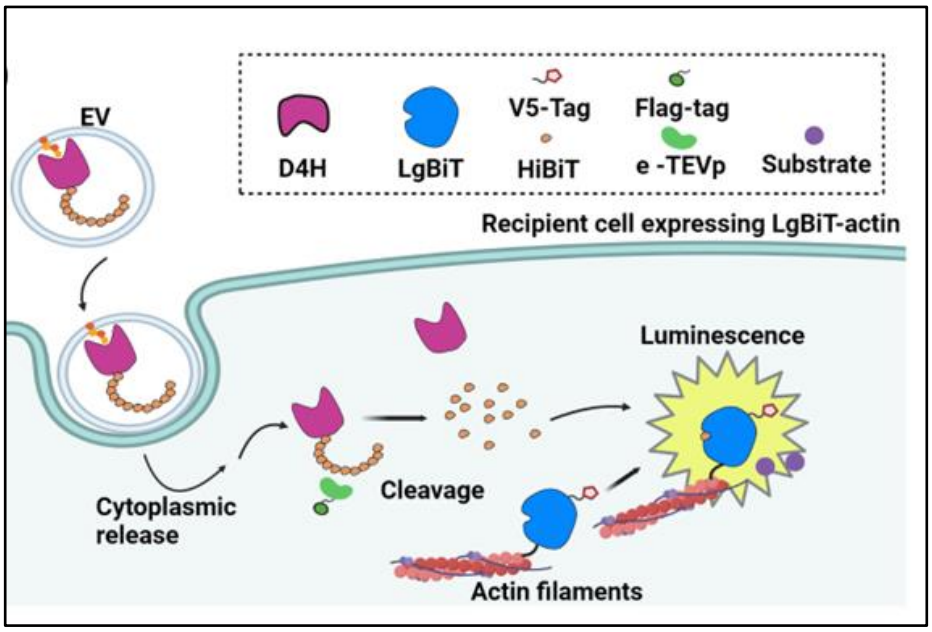

Fig 3.0.1: Basic principle of protein delivery by D4-EVs. A schematic model of D4-EVs internalization and cargo release in recipient cells. EVs from donor cells contains $D4_{YDA}$-12 × HiBiT cargo is internalized into recipients expressing LgBiT retained in cytoplasm by fusion with actin. After internalization and cargo release of the engineered EVs, eTEVp cleaves the tandem HiBiT into single peptides. The HiBiT complements to LgBiT fragment to form a full-length NanoLuc luciferase.

EV cargo delivery has been considered a rare biological event that requires a stable and highly sensitive but short time assay to capture this intracellular event. Owing to this, we utilized the protein-fragment complementation assay (PCA) of a small luciferase NanoKAZ/NanoLuc to detect the intracellular release of the cargo of D4-EVs (Dixon et al., 2016). This PCA approach uses complementary fragments of a luciferase enzyme to monitor protein-protein interactions in living cells (Ohmuro-Matsuyama, Chung, & Ueda, 2013). The NanoKAZ/Nanoluc is a luciferase enzyme derived from *Oplophorus gracilirostris* - a deep sea luminous shrimp (Tomabechi et al., 2016). NanoKAZ is a full-length 19kDa luciferase unit that can be further spitted into a NanoBiT unit consisting of LargeBit (LgBiT ,18kDa) and SmallBit (SmBiT, 1.3kDa) peptide also referred to as HiBiT (Fig. 3.0.2).

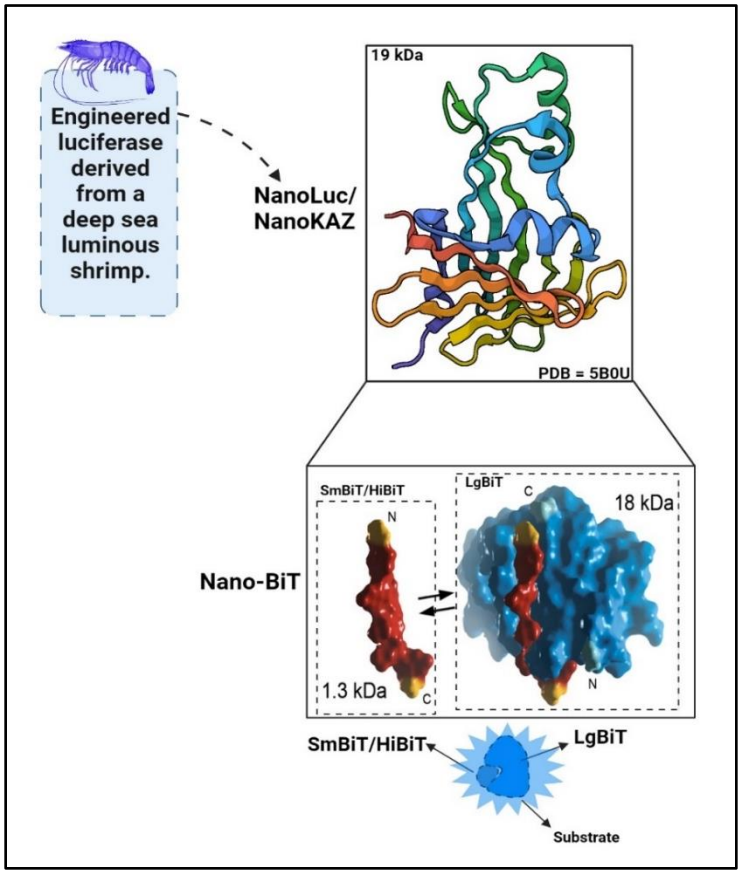

Fig 3.0.2: Structure and complementation activity of 19kDa NanoLuc/NanoKAZ.

When LgBiT and HiBiT are reconstituted or brought in proximity because of PCA, the luciferase enzyme catalyses a bioluminescent reaction and generates a luminescent signal that can be quantified using a luminometer. In this section, we established models of donor and recipient cells necessary for secreting engineered D4-EVs and detecting content release of D4-EVs respectively.

3.1 Materials and Methods

3.1.1 Plasmids

For the generation of NanoKAZ/NanoLuc PCA, the small bit with high affinity (HiBiT) cDNA was designed as 12 tandem repeat sequences each of which flanked by TEV protease recognition sites. The 12 × HiBiT sequence was constructed by phosphorylation and annealing of oligo DNAs, fused to N and C terminuses of D4-YDA and CD9 cDNAs, respectively, and cloned into pPB split-PAC vectors (Horikawa, Sabe, & Onodera, 2021). Stag was also added for antibody detection. NanoKAZ/NanoLuc large bit (LgBiT) cDNA was obtained by gene synthesis service, fused to cDNAs encoding β-actin and V5 tag, and cloned into a pPB split-PAC vector. For cleavage of the tandem HiBiT peptides, cDNA encoding e-TEV protease (Denard et al., 2021) was obtained by gene synthesis service, fused to Flag tag and cloned into a pPB split-PAC vector. All these split-PAC vectors were constructed using a backbone of doxycycline-inducible pPB vector (Onodera, Nam, Horikawa, Shirato, & Sabe, 2018; Yusa, Zhou, Li, Bradley, & Craig, 2011).

3.1.2 Immunofluorescence of recipient cells

Cells were fixed in 4% Paraformaldehyde (PFA) at RT for 10 min and washed with PBS. The cells were permeabilized with 0.2% Triton in PBS and blocked with 5% bovine serum albumin (BSA) in PBS at RT for 1 h. Cells were washed with PBS and incubated with primary antibodies in 5% BSA in PBS at 4°C overnight. Cells were washed with PBS and incubated with Alexa Fluor-conjugated secondary antibodies at RT for 1 h. Nuclear DNA was stained with 4’,6-diamino-2-phenylindole (DAPI). Images were acquired by a Leica TCS SP8 confocal microscope (Leica Microsystems).

3.1.3 Viability assay by CCK-8 Assay

Viability of cells treated with HiBiT EVs or concentrated EVs by 4XPEG buffer was determined by Cell Counting Kit (CCK-8; Dojindo). Equal number of cells was seeded into 96-well plate and treated with appropriate volumes and concentrations of EVs in CM or PEG-EVs respectively for up to 48hrs. Afterwards, CCK-8 solution was added to cells for 1h at 37℃. Cell viability was thereafter measured at an absorbance of 450nm using Multiskan™ GO Microplate Spectrophotometer (Thermo Fisher Scientific).

3.1.4 VSV-G transfection

7e5 donor cells were seeded on a 10 cm dish and induced with 50 ng/ml of doxycycline after adherence. 24 h after induction, cells were transfected with a mix of 500 µl of Optimem, 10 µg of VSV-G plasmid, and 20 µl Avalanche Following cellular transfection after 24 h, cells were washed with PBS twice and replaced with 5 ml of medium containing exosome-depleted serum and incubated with 50 ng/ml of doxycycline in 37°C for 48 h. Donor cell supernatant was thereafter harvested and prepared for EV isolation as previously described in *1.1.3.*

3.1.5 Protein delivery assay.

For the protein delivery assay, recipient cells seeded on 96-well plates were induced with doxycycline (50 ng/ml), and cells were pre-treated with 1 nm of DrkBiT peptide to quench possible extracellular luminescence and incubated with equal volumes of HiBiT-EVs in CM or 10-20µg of concentrated EVs for up to 24 h in 37°C. After incubation, medium was aspirated, and cells were washed thrice with empty medium. Medium containing nanoluc substrate (Vivazine) was applied into cells for 1 h at 37°C. Nanoluc luminescence signal was measured using a Clariostar® micro-plate reader (BMG LABTECH) in a bottom-optic mode and activity was normalized to control samples.

3.2 Results

3.2.1 Detection of LgBiT-actin and eTEVp fusion in model of recipient cells

To quantitatively determine the cytoplasmic distribution of D4-EVs, we establish a recipient cell model based on split NanoKAZ/Nano-luciferase reporter system (Fig 3.2.1 A). In the recipient cells, LgBiT was fused to a permanent cytoskeletal actin monomer to minimize the unintended secretion of LgBiT into the extracellular space (Teo et al., 2021). To release EV-cargo into recipient cells, we constructed tandem repeats of HiBiT connected to with a recognition sequence of enhanced tobacco etch virus protease (eTEVp) and co-expressed eTEVp in the recipient cells together with LgBiT. Our results show expression of LgBiT-actin and eTEVp fusion by immunoblotting (Fig 3.2.1B) and the localization of proteins were confirmed by V5 and Flag immunostaining for LgBiT-actin and eTEVp respectively (Fig 3.2.1C).

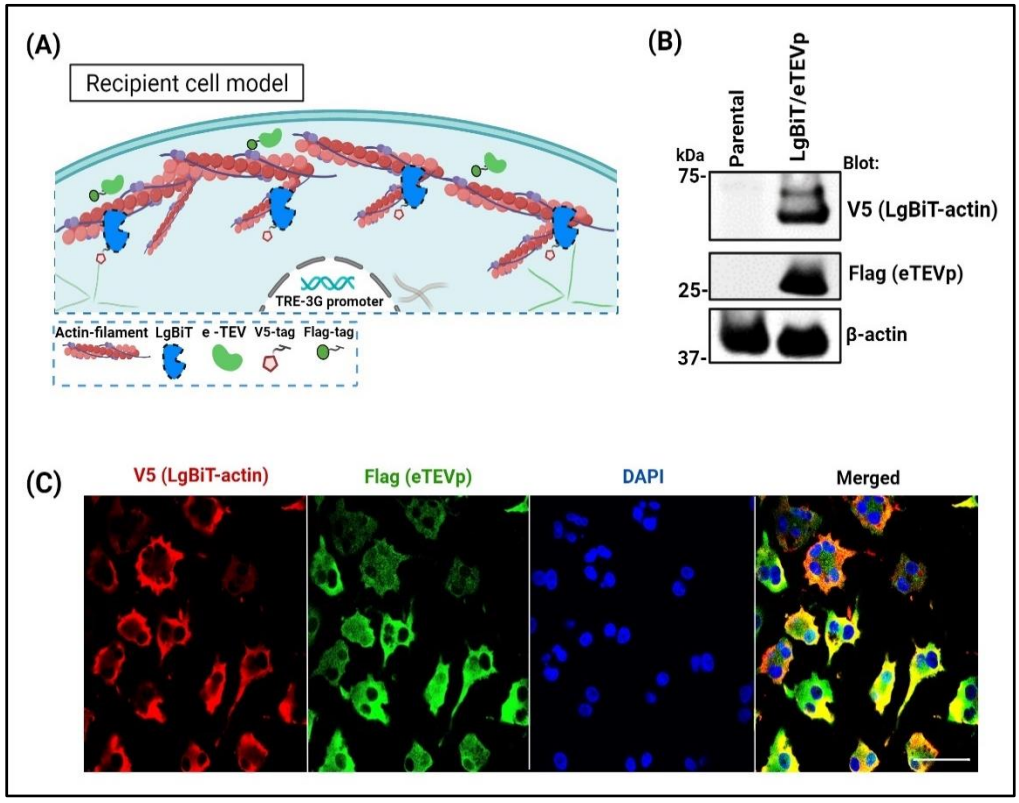

Fig 3.2.1: V5-LgBiT-actin and Flag-eTEVp and are co-expressed in recipient cells. (A) Model of recipient cell for detecting EV cargo release B) Co-expressing V5-LgBiT-actin and Flag-eTEVp were detected in U87-MG cells by western blotting using indicated antibodies. (C) LgBiT and eTEVp expression in U87-MG recipient cells examined by confocal microscopy using indicated antibodies. Red, V5-LgBiT-actin; green, Flag-eTEVp; blue, DAPI (nuclei). Bar, 25 µm.

3.2.2 HiBiT fusion expression in engineered donor cells

To confirm the expression of tandem repeats of HiBiT peptide, U87MG (Fig 3.2.2) donor cells were seeded for EV isolation. Immunoblotting analysis show that both 12X repeats of HiBiT are effectively loaded into EVs by fusion to CD9 and $D4_{YDA}$.

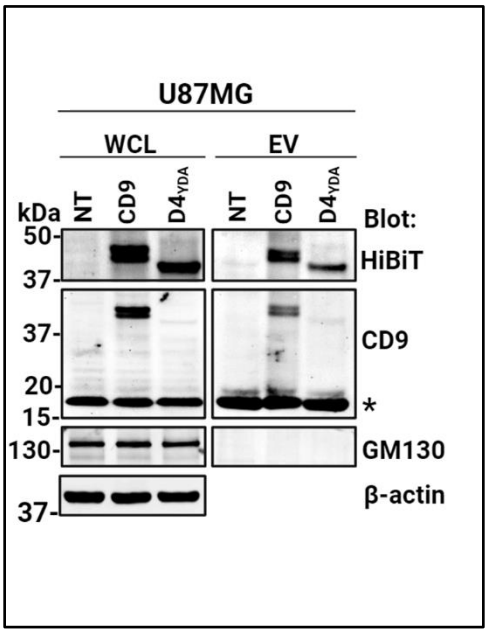

Fig 3.2.2: Characterization of HiBiT fused proteins in donor cells. (A**)** Cell lysates and EV fractions of stable U87MG donor cells expressing CD9 or $D4_{YDA}$ fused with 12× tandem repeat of HiBiT peptides were subjected to immunoblotting analysis using indicated antibodies (Asterisk indicates endogenous CD9).

3.2.3 Effect of TEVp-mediated cleavage HiBiT-peptide

To ascertain the effective cleavage of HiBiT by eTEVp (Fig 3.2.3A), we constructed 12x tandem HiBiT connected with non-cleavable (NC) eTEVp target sequence (ENLEHV). Plasmids encoding the tandem HiBiT peptides with NC or cleavable (C) sequence were transfected into recipient cells stably expressing LgBiT-actin and eTEVp (Fig 3.2.3B) and C-HiBiT was abrogated in the recipient cells suggesting the efficient cleavage of C-HiBiT by eTEVp. In this experimental setup, the expression levels of LgBiT and eTEVp are expected to be similar between two conditions (NC vs C). We confirmed that although the NC version produced somewhat higher bioluminescence than the negative control (about 3.5 fold, statistically significant only when directly compared using T-test), the C version showed

significantly higher intensity then the NC version (about 42 fold). Expression level and/or stability of the NC version were rather higher compared to the C version, showing that the significant increase in bioluminescence was due to eTEVp-mediated cleavage and release of HiBiT peptides, but not the difference in their expression levels.

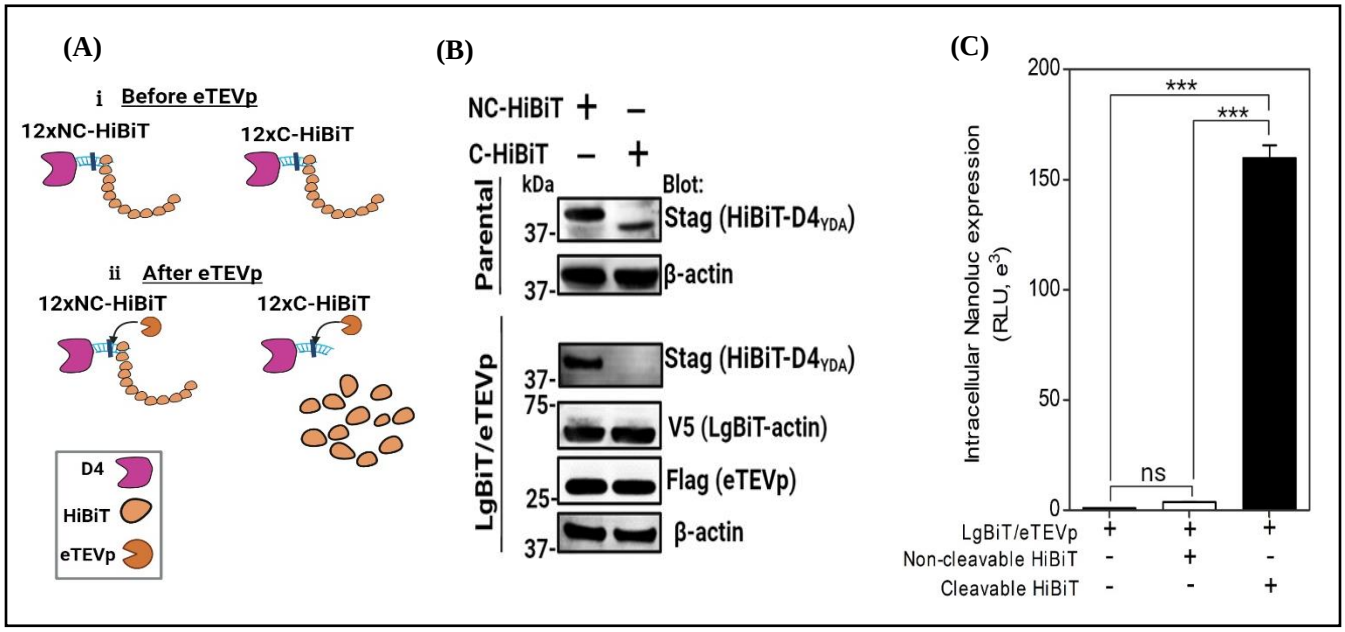

Fig 3.2.3: Effect of TEVp-mediated cleavage HiBiT-peptide. (A**)** Schematics of the effect of eTEVp on Non cleavable and cleavable HiBiT peptides. (B) HEK-293T cells were transfected with plasmid DNAs encoding either 12 × tandem HiBiT connected with non-cleavable (NC) or cleavable (C) TEVp target sequences. Parental cells (without cleavage) and recipient cells (LgBiT/eTEVp, with cleavage) were used. Protein expressions were analyzed by western blotting with the indicated antibodies. (C) Quantification of intracellular NanoKAZ/NanoLuc PCA with or without TEVp-mediated cleavage on 12 × tandem HiBiT peptide. HEK-293T recipient cells were treated with 50 ng/ml of doxycycline to induce LgBiT/eTEVp expression and then transfected with plasmid DNAs encoding either non-cleavable or cleavable 12 × tandem HiBiT. Luminescence was measured in the presence of Vivazine. The graph shows mean ± SEM from six biological replicates and the background signal was subtracted from each value. Statistical analysis was performed using one-way ANOVA adjusted by Tukey's test. ns (not significant) denotes $P > 0.05$ and *** $P < 0.0001$.

3.2.4 Detection of reconstituted active luciferase complex intracellularly by PCA

To further confirm the complementation activity of LgBiT and HiBiT peptide to form active luciferase complex, we transiently transfected HiBiT-encoding plasmids in U87MG recipient cells (Fig. 3.2.4A) and induced reporter gene expression with doxycycline. Our results demonstrate that only when HiBiT and LgBiT are co-expressed together, a strong Nanoluc expression is formed by luciferase PCA (Fig 3.2.4B).

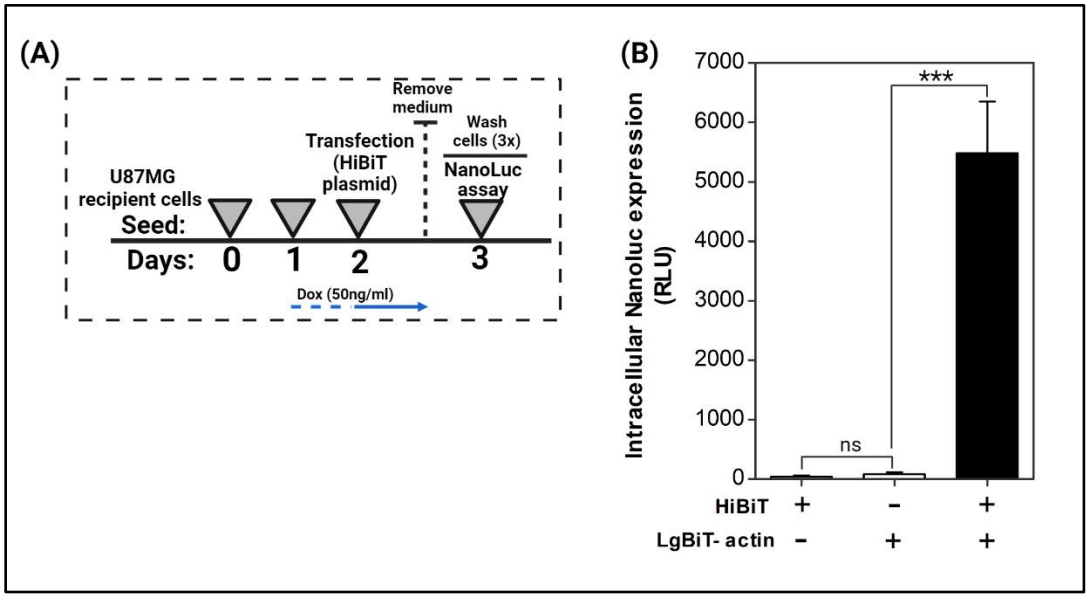

Fig 3.2.4: Transient transfection of HiBiT plasmid into LgBiT/eTEVp recipient cells. (A**)** Intracellular NanoKAZ/Nanoluc PCA in U87 LgBiT-eTEVp cells after HiBiT transfection. Recipient cells were treated with 50 ng/ml of doxycycline (+) or vehicle (-) to induce the expression of LgBiT and eTEVp constructs (A), and then transfected with plasmid encoding HiBiT. Luminescence signal was measured in the presence of Vivazine. Graph represents mean ± SEM from 3 independent experiments. Statistical analysis was performed using one-way ANOVA adjusted by Tukey's test. ns (not significant) denotes $P > 0.05$ and *** $P < 0.001$.

3.2.5 Inhibition of extracellular NanoKAZ/NanoLuc formation by DrkBiT peptide

The EV protein delivery assay by split NanoKAZ/Nanoluc is posed with the challenge of detecting unwanted luminescence signal that arises from complementation of non-encapsulated HiBiT EVs with secreted extracellular LgBiT (Somiya & Kuroda, 2021a). To inhibit the formation of extracellular luciferase complex, we applied DrkBiT, a small membrane-impermeable peptide and competitive inhibitor of LgBiT (Fig 3.2.5A) that inactivates luciferase activity into the medium of culture assay (Evans et al., 2019). Our results show that in the presence of 1µM DrkBiT, extracellular luminescence was sufficiently suppressed. In contrast, culture medium without DrkBiT shows increased activity of luminescence signal (Fig 3.2.5B).

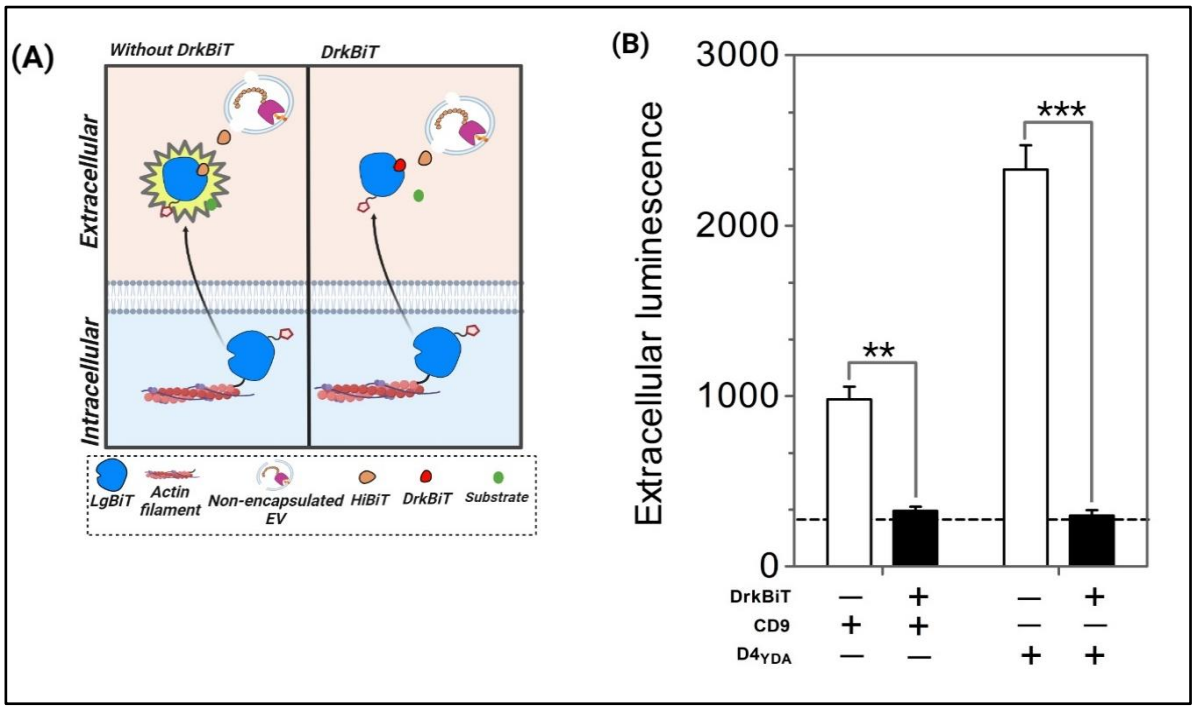

Fig 3.2.5: DrkBiT minimises formation of extracellular NanoKAZ/NanoLuc. (A) Model of extracellular NanoKAZ/Nanoluc formation with or without DrkBiT peptide. (B**)** Inhibitory effect of 1µM of DrkBiT peptide on complementation activity of split Nanoluc extracellularly. Medium from U87MG recipient cells and donor cells were separately extracted from cultured cells, centrifuged at 2000g for 30mins to remove cellular debris and mixed at equal volumes in a 96-well plate. 1µM of DrkBiT was pre-treated into the recipient cell medium just before

adding donor cell supernatant and incubated with nanoluc substrate biz-coelenterazine. Luminescence signal was obtained, and horizontal line represents the average background signal in empty medium. Graph showed mean ± SEM from three independent experiments. Statistical analysis was performed by student t-test, **P = 0.0011 and ***P = 0.0002

3.2.6 Encapsulation of VSV-G in EVs of engineered donor cells

To modify donor cells for secreting EVs capable of membrane fusion with recipient cells, we transiently transfected donor cells in (Fig 3.2.2) with VSV-G plasmids. VSV-G has been reported to facilitate EV-membrane fusion and enhancing cargo delivery of EVs (Albanese et al., 2021; Somiya & Kuroda, 2021b). According to Fig (3.2.6), VSV-G was detected in EV fractions of donor suggesting the display of VSV-G on the surface of EVs. However, the expression of VSV-G was slightly abrogated in donor cells when compared to mock (parental cells).

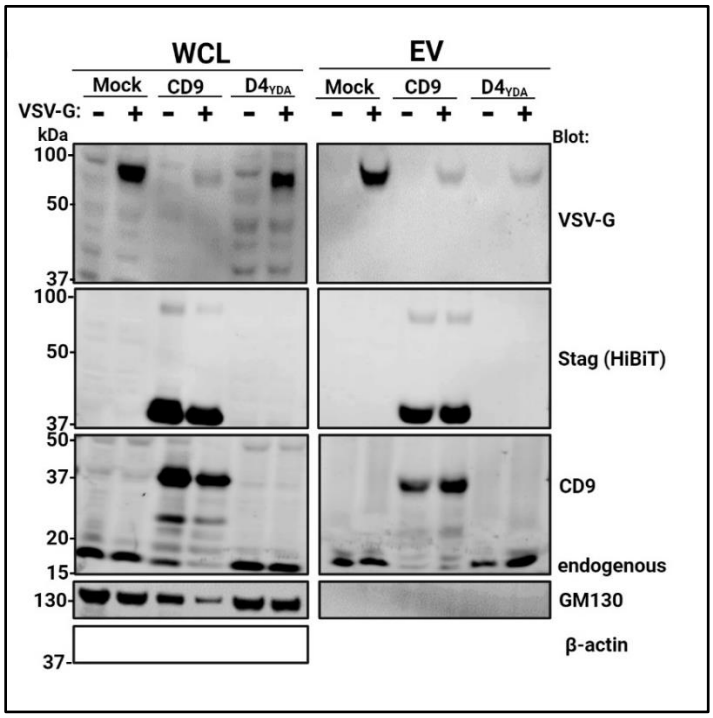

Fig 3.2.6: Detection of VSV-G in HiBiT engineered donor cells by western blot (A) Immunoblotting of lysate and EV fractions of U87-MG donor cells expressing 12x HiBiT tagged to either CD9 or $D4_{YDA}$ for detection of VSV-G and EV marker proteins using indicated antibodies.

3.2.7 Intracellular delivery of HiBiT-tagged cargo between $D4_{YDA}$-EVs vs CD9-EVs and enhanced by VSV-G

EVs can be taken up by recipient cells, but the intracellular cargo delivery of EVs into recipient cells still lacks plausible evidence. This is partly due to the lack of reliable or sensitive assays for determining functional readout of EV cargos once released into the cytosolic region of recipient cells (Somiya, 2020). Having ascertained that D4-EVs can be internalized by recipients cells, we therefore investigated its ability for protein delivery. We utilized previously described split NanoKAZ/Nanoluc reporter system as stated in *3.0* for evaluating cargo-releasing of $D4_{YDA}$-EVs and compared with CD9-EVs. Isolated EVs from donor cells (MDA-MB-231 and U87MG) transfected with or without VSV-G and later applied to U87MG recipient cells (Fig 3.2.7A). Our result shows that EVs displaying VSV-G induces Nanoluc expression after a treatment time of up to 24hrs in recipient cells, suggesting the effectual release of HiBiT peptide from EVs to bind with intracellular LgBiT (Fig. 3.2.7B-C). In contrast, EVs without VSV-G did not elicit sufficient luminescence signal indicating the absence of luciferase activity in recipient cells. Most importantly, cargo release and protein delivery efficiency between $D4_{YDA}$-EVs and CD9-EVs are almost equivalent as there are no statistically significant differences between their relative luminescence units. We also confirm that, EVs from different donor cell (MDA-MB-231) transferred into a different recipient cell (U87MG) can mediate effective protein delivery (Fig. 3.2.7B). The experimental evidence from these results indicates that functional delivery of EV cargo can only be mediated by VSV-G in facilitating EV-membrane fusion. Further studies are required to assess the effect of delivery enhancers such as endosome-destabilization reagents on EV-cargo delivery using this assay.

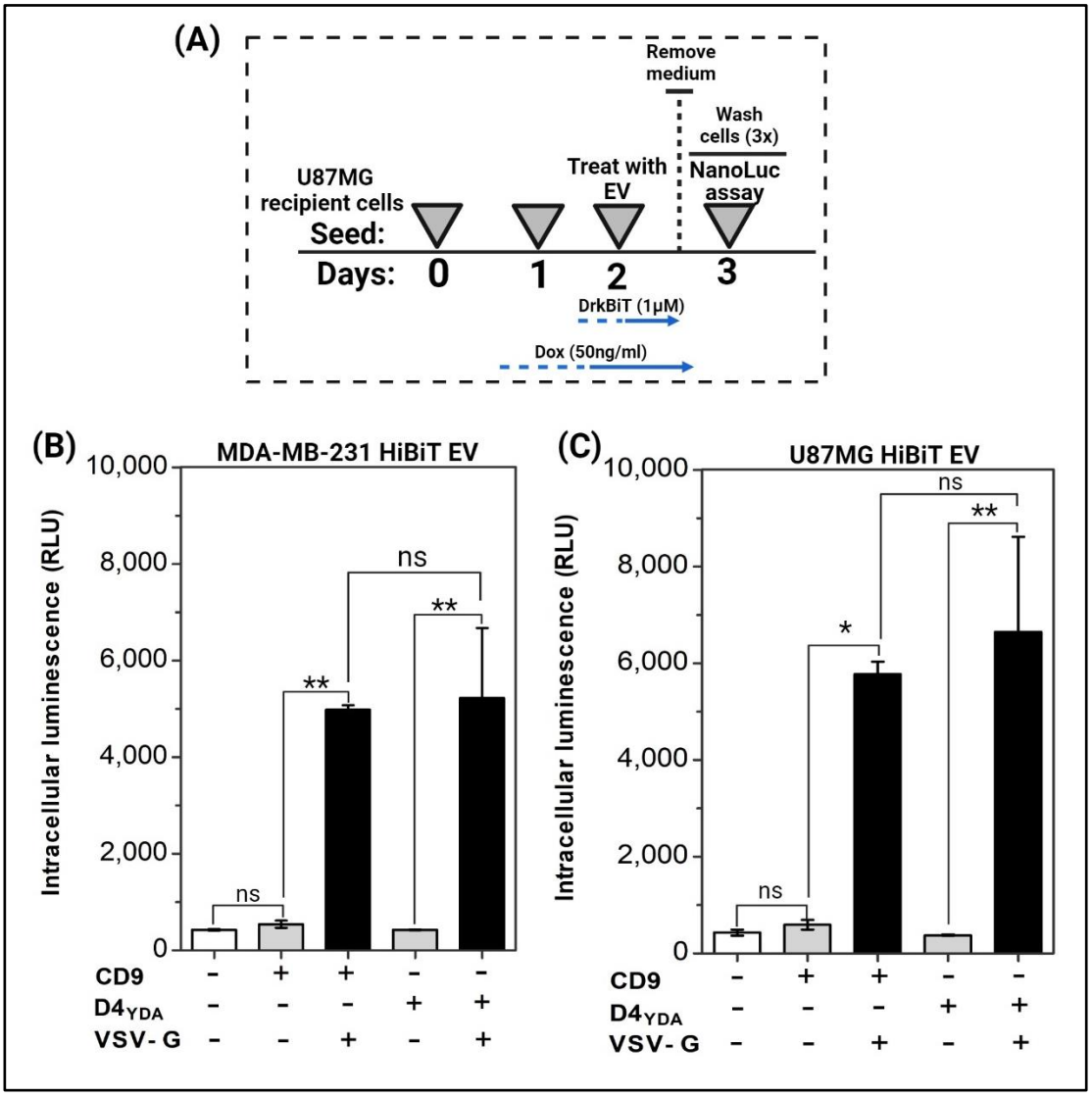

Fig 3.2.7: Intracellular protein delivery of HiBiT-tagged EVs assisted with VSV-G (A) Experimental set-up for protein delivery assay. (B-C) NanoKAZ/Nanoluc PCA in recipient cells treated with EVs. Intracellular delivery of HiBiT-tagged cargo between $D4_{YDA}$-EVs vs CD9-EVs. Concentrated EVs from donor HiBiT cells; MDA-MB-231 (B) and U87MG (C) were applied to recipient cells expressing the LgBiT and eTEVp constructs for up to 24 h after DrkBiT incubation. Luminescence was measured in the presence of Nanoluc substrate (Vivazine). Graph shows mean ± SEM from six biological replicates. Statistical analysis was performed by one-way ANOVA, adjusted with Tukey's post hoc test. ns (not significant) denotes $P > 0.05$, * $P < 0.05$, ** $P < 0.05$.

3.2.8 Cytotoxic analysis of recipient cells treated with HiBiT-EVs by CCK-8 assay.

The relative cell viability of U87-MG recipient cells treated with EV was determined using CCK-8 and results normalized to untreated cells (Fig 3.2.8A). The results show no statistically significant difference between cells treated with CD9-EVs or $D4_{YDA}$-EVs and untreated cells (Fig 3.2.8B). However, there was a statistically significant difference in recipient cells treated with VSV-G coated CD9-EVs or $D4_{YDA}$-EVs compared to untreated cells suggesting that the presence of VSV-G may mediate some effects on recipient leading to a decrease in viability.

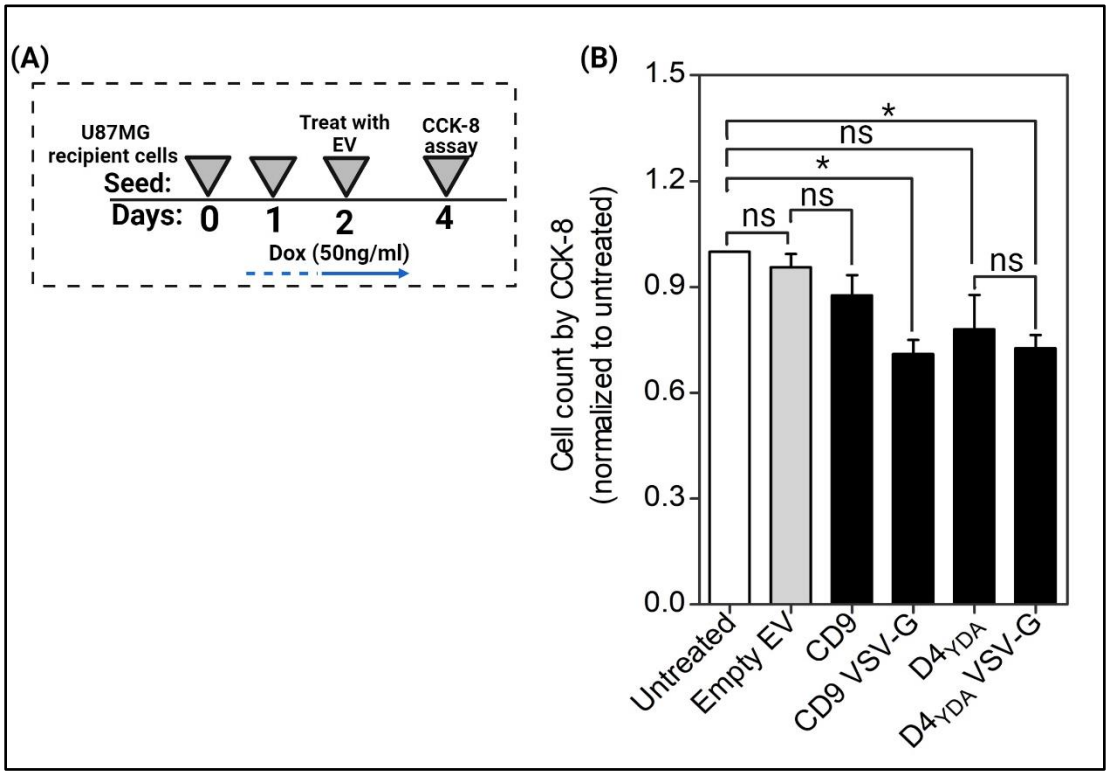

Fig 3.2.8: Viability of cells after treatment with HiBiT-EVs (A) Experimental set-up for determining viability of recipient cells by CCK-8 assay after EV treatment. (B) Viability of recipient cells treated with EV measured 48hours post treatment. Viability was determined using CCK-8. Graph shows the mean ± SEM (n = 3) from six biological replicates with results normalized to untreated cells. Statistical analysis was performed by one-way ANOVA, adjusted with Tukey's post hoc test. ns (not significant) denotes $P > 0.05$, * $P < 0.05$.

3.3 Discussion

3.3.1 Reporter systems for EV cargo delivery

There are several reporter systems that have been developed for investigating the cytoplasmic distribution of EV cargo (Han & Qin, 2022). The cell cytosol's is highly dynamic owing to its complex intracellular feedback networks and the quantitative measurement of dispersed biological molecules within the cytosol requires a highly sensitive experimental technique (Luby-Phelps, 2013; Molines et al., 2022). In this section, we leveraged on ultrasensitive split-luciferase technology to assess EV cargo discharge since the biological delivery of EV cargo into the cytoplasmic environment of cells has been considered a rare event (Dixon et al., 2016; Somiya, 2020). Previously, Teo et a., used split-luciferase to quantify the cytosolic delivery of some cell-penetrating peptides (CPP) (Teo et al., 2021). However, their assay could only detect CPP's cargo in recipient cells after endosomal escape has occurred. Split EGFP-luciferase fusion proteins were also used to quantitatively measure cellular uptake of EVs, but this method could not distinguish between EV uptake and EV cargo release (Toribio et al., 2019). Split-luciferase has also been used to measure the membrane fusion event between virus-like particles (VLP) and EVs (Kicmal, Qing, Hawkins, Wilcox, & Gallagher, 2023). The VLP-EV fusion may have demonstrated transfer of cargo across the plasma membrane, but this assay is cell-free and does not provide evidence for direct cytosolic delivery. Aside from split-luciferase, other EV cargo delivery assay such as the CROSS-FIRE system (de Jong et al., 2020) and the Cre-LoxP reporter system (Zomer et al., 2015; Zomer, Steenbeek, Maynard, & Van Rheenen, 2016) were used to measure functional readout of EV cargo-release. The CROSS-FIRE system employs CRISPR/Cas9 to visualize at a single cell-resolution the transfer of single guide RNA (sgRNA) which only activates fluorescence in recipient cells after delivery has taken place. While the CROSS-FIRE may be highly sensitive for small RNA transfer, it requires five days of EV co-culture with recipients for effective functional readout. Likewise, the Cre-LoxP system enables transfer of large Cre mRNA molecules or Cre proteins and activates fluorescent protein in recipient reporter cells after functional cargo delivery. The Cre-LoxP system has been reported to be suitable for in-vivo applications rather in-vitro.

Recently, Somiya et al., developed an EV cargo delivery (EVCD) assay also based on split luciferase to measure the kinetics of cargo delivery by EV in living cells. While this assay was successful in visualizing EV cargo delivery in real time, tetraspanin (CD9/63/81) was deployed as machineries for cargo loading of split-luciferase into EV. The controversies surrounding tetraspanins are enormous as previously stated in *1.0*, so our study focused more on comparing EV cargo delivery efficiencies between $D4_{YDA}$ and CD9. Prior to this, we first characterized the expression and localization of split luciferase fragment LgBiT in our recipient cell model (Fig. 3.2.1) and further confirmed its complementation activity in forming active full-length luciferase complex upon LgBiT-HiBiT binding (Fig. 3.2.4). Our results shows that LgBiT localises within the cytosol of recipient cells and is co-localized with eTEVp for cleaving HiBiT peptide from EV after membrane fusion with the recipient cells. We also demonstrated that donor cells release engineered EVs containing tandem repeats of HiBiT peptide as seen in Fig. 3.2.2. 12x tandem repeat was slightly enriched than 8x tandem repeat design of HiBiT peptide and we selected the 12x-HiBiT peptide expressed in donor cells for the EV-cargo delivery assay. Somiya et al., had used a single HiBiT peptide per CD9 protein for EV cargo loading (Somiya & Kuroda, 2021a), while we increased the loading amount of HiBiT peptide fused to either $D4_{YDA}$ or CD9 to the order of 12times. This strategy is expected to further enhance functional readout of EV cargo.

A challenge with the split-luciferase for monitoring EV cargo delivery is the detection of non-specific or high background luminescence signals that arises from extracellular secretion of LgBiT and binding with non-encapsulated HiBiT peptide in EVs. This binding can form full-length Nanoluc that can be further endocytosed into the recipient cells and detected as a false signal in functional read out of EV cargo (Teo et al., 2021). Just as with other studies investigating EV cargo release, we introduced DrkBiT into recipient cells to inhibit possible extracellular signals and our result shows that DrkBiT quenches to a reasonably extent the formation of extracellular full-length Nanoluc (Fig 3.2.5a). As DrkBiT is membrane-impermeable, we tested the cytotoxic possibility of DrkBiT incubation into recipient cells and our results shows that was no statistically significant differences between untreated cells and cells treated with DrkBiT. Unexpectedly, the viability of recipient cells decreases in a

time-dependent culture (Fig 3.3.1), and this may result from culturing recipient cells in exosome depleted-serum which is our strategy to reduce competition between engineered EVs and serum-associated exosomes. Further studies are required to develop a recipient cell model in which unwanted extracellular luminescence can be self-inactivated just before performing the EV cargo delivery assay, as this will improve the robustness and accuracy of EV cargo delivery in both in-vitro and for in-vivo applications especially where DrkBiT cannot be applied.

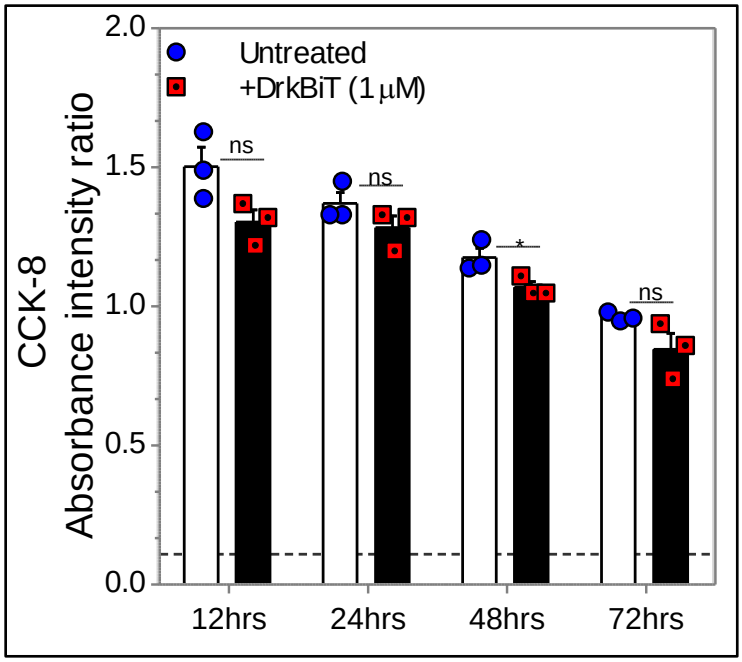

Fig 3.3.1: Viability of recipient cells after DrkBiT treatment (B) Viability of recipient cells treated with DrkBiT measured 48hours post treatment. Viability was determined using CCK-8. Graph shows the mean ± SEM (n = 3) of three independent experiment. Statistical analysis was performed by t-test. ns (not significant) denotes $P > 0.05$, * $P < 0.05$.

3.3.2 The role of VSV-G in EV cargo delivery

In the EV cargo transfer hypothesis, direct EV-to-cell membrane fusion has been proposed has the first biological step before content release of EV into cell's cytosol can take place (Kalluri & LeBleu, 2020; Somiya, 2020). After membrane fusion, it is expected that the internal lumen of the EV membrane fuses with the outward membrane of the target cell making both membrane continuous and thereafter, the contents of EVs are released into the cytosolic region (Prada & Meldolesi, 2016). However, for EV-to-cell membrane fusion to occur, EV needs to overcome the energy barrier that exists within the extracellular space thus requiring the need for fusion proteins to mediate direct fusion with the membrane of target cells. As a proxy to EV, several studies have reported the role of fusogenic VSV-G in mediating such processes and concluded that EV does not possess the inherent capacity to deliver cargo directly into recipient cells (Fig. 3.3.2). except assisted with VSV-G (Albanese et al., 2021; Meyer et al., 2017; Somiya & Kuroda, 2021b; Votteler et al., 2016). Our result was consistent with others, and we only confirmed the release of EV coated with VSV-G when applied into recipient cells (Fig. 3.2.7). A statistically significant increase in intracellular luminescence in the groups of HiBiT-EVs coated with VSV-G was detected in recipient cells after a treatment time of up to 24hrs compared with non-coated HiBiT-EVs. Other studies also reported that longer incubation period does not contribute to cytoplasmic cargo delivery as EV-membrane fusion and delivery is a rapid event (Le Blanc et al., 2005; Somiya & Kuroda, 2021a). Moreover, we also confirmed that EVs indeed display VSV-G as detected by immunoblotting of engineered donor cells (Fig 3.2.6). Furthermore, we treated recipient cells EVs in CM and our results show that EVs in CM are not significantly sufficient to induce intracellular luminescence whether they are coated with or without VSV-G (data not shown). This might suggest a need for concentration of EVs for use in the delivery assay. Overall, we have demonstrated an equivalent protein delivery efficiency between $D4_{YDA}$ and CD9. Despite the relatively lower uptake of mScarlet-I-$D4_{YDA}$-EVs in Fig 2.2.3, our protein delivery assay shows that HiBiT-$D4_{YDA}$-EVs can bio-actively deliver cargo in relative capacity to CD9-EVs.

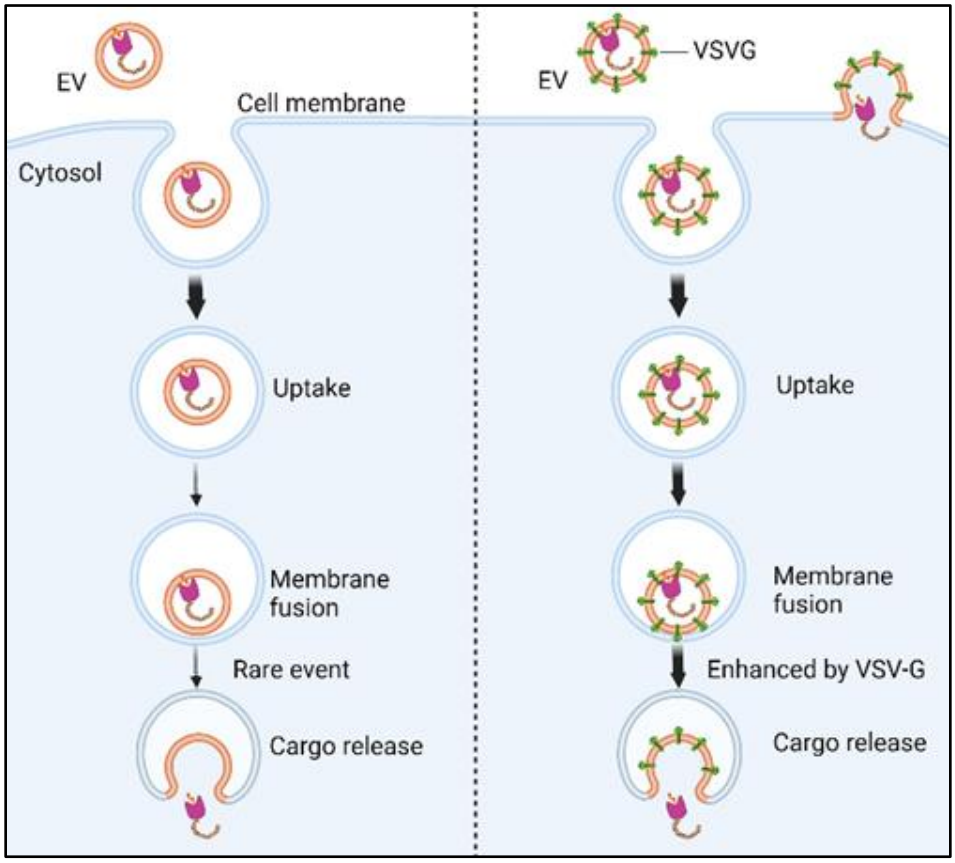

Fig 3.3.2: A scheme of the effects of VSV-G on EV cargo release.

Summary and Conclusion

Experimental Finding 1

The conclusion of results discussed in this section are briefly outlined below:

- D4 of PFO successfully loads TagRFP into EVs and POIs are detected in multiple cell types including cholesterol-enriched glioblastoma cells.
- Mutated D4-series are likewise accumulated in EVs.
- D4-series localizes to intracellular vesicular structures and in plasma membrane.
- D4-EVs are efficiently captured and detected by CD9-positive EVs, which is considered as ectosome.

Experimental Finding 2

The conclusion of results discussed in this section are briefly outlined below:

- mScarlet-I reveals intrinsic brightness in $D4_{YDA}$ localization to plasma membrane and vesicular structures when compared to other fusion tags.
- mScarlet-I enhances fluorescence detection when used to label EVs by $D4_{YDA}$.
- mScarlet-I can be loaded into EVs either by CD9 or $D4_{YDA}$ at equivalent efficiency.
- $D4_{YDA}$-EVs can be internalized in cytosolic region of recipient cells.
- CD9-EVs are captured at the surface of cells, thus promoting uptake of specific CD9-EVs.

Experimental Finding 3

The conclusion of results discussed in this section are briefly outlined below:

- $D4_{YDA}$-EVs are capable of intracellular protein delivery with equivalent efficiency to CD9 EVs.

- $D4_{YDA}$-EVs releases POIs into recipient cell's cytosol only when EVs are coated with fusogenic VSV-G.

The current understanding regulating EV cargo delivery into the cytoplasmic environment of recipient cells has been proposed, however the system for detecting this cargo release is technically elusive. Given the biological and clinical potentials of EVs, it is imperative to develop an efficient technology for assessing the release of EV contents into recipient cells.

In this present study, we first developed a unique strategy to recruit POIs into EVs through a cholesterol-binding domain D4. Our results show D4 loads POI into EVs of several cell lines and the developed mutant of D4 aimed at improving its binding affinity to cholesterol are also loaded into EVs. We also demonstrate D4 has an equivalent cargo loading efficiency with widely used CD9 tetraspanin. Furthermore, we confirm that D4-EVs can be internalized by recipients cells with localization to cytosolic region and possible endosomal structures.

Also, we report using split-luciferase technology that D4-EVs possess the capacity for intracellular protein delivery with equivalent efficiency to that of CD9-EVs when assisted with fusogenic proteins.

As a contribution to knowledge, we propose that D4 can be used as a viable candidate for EV protein loading and delivery. Our studies pave the way for developing novel tools for monitoring EV-mediated cell-cell communication, which could be further used to deliver bioactive cargo for therapeutic and diagnostic applications. Further studies are required to enhance D4's loading ability by optimizing its binding affinity to cholesterol and regulate the amount of POI into EV especially in the case of precision medicine for drug delivery. Finally, our assay needs to be validated to exclude the luminescence artefacts that may interfere with the EV-cargo delivery.

Acknowledgements

This research was funded by Grant-in-Aid for Scientific Research provided by the Japanese Society for Promotion of Science, SENSHIN Medical Research Foundation, Sugiyama Chemical & Industrial Laboratory, and supported in part by Global Center for Biomedical Science and Engineering (GCB), Hokkaido University. The findings presented in this thesis represent a compilation of research outcomes conducted under the supervision of Associate Professor Yasuhito Onodera from the Laboratory of Molecular and Cellular Dynamics Research, Graduate School of Biomedical Science and Engineering at Hokkaido University.

First, I am deeply thankful to my thesis advisor Dr. Yasuhito Onodera, for his unwavering support and mentorship. His expertise, guidance, and constructive feedback have been instrumental in shaping the direction and quality of my research. Thank you for being an 'angel' to me. Also, I am forever indebted to MEXT, Distinguished Professor Hiroki Shirato and Associate Professor Jin-Min Nam for granting me the opportunity to study radiation biology related-research and for the multiple fellowships they have provided which have lightened my financial burden and allowed me to wholeheartedly focus on research. **(本当にありがとう。すべてに感謝している).**

Second, I extend my sincere gratitude to members of my thesis evaluation committee for their expertise and diverse contributions towards the refinement and completion of this study.

Third, I would like to thank all students, members, and technical staffs of the Laboratory of Molecular and Cellular Dynamics Research, administrative staffs at GCB and the Graduate School of Biomedical Science and Engineering at Hokkaido University for providing a peaceful academic environment for study.

Finally, my heartfelt appreciation and profound gratitude goes to my lovely parents back home in Nigeria for their prayers, support, encouragement, and profound belief in me. I wouldn't have gone this far in life without my Dad and Mum. **(Ese pupo, modupe).**

In conclusion and most importantly, my reverence and honour belong to God for giving me the strength in my deep moments of weakness, shame, and failure.

References

Albanese, M., Chen, Y. F. A., Hüls, C., Gärtner, K., Tagawa, T., Mejias-Perez, E., … Hammerschmidt, W. (2021). MicroRNAs are minor constituents of extracellular vesicles that are rarely delivered to target cells. In *PLoS Genetics* (Vol. 17). https://doi.org/10.1371/journal.pgen.1009951

An, Z., & Weiss, W. A. (2016). Cholesterol: An Achilles' Heel for Glioblastoma? *Cancer Cell*, *30*(5), 653–654. https://doi.org/10.1016/j.ccell.2016.10.011

Anand, S., Foot, N., Ang, C. S., Gembus, K. M., Keerthikumar, S., Adda, C. G., … Kumar, S. (2018). Arrestin-Domain Containing Protein 1 (Arrdc1) Regulates the Protein Cargo and Release of Extracellular Vesicles. *Proteomics*, *18*(17), 1–6. https://doi.org/10.1002/pmic.201800266

Baietti, M. F., Zhang, Z., Mortier, E., Melchior, A., Degeest, G., Geeraerts, A., … David, G. (2012). Syndecan-syntenin-ALIX regulates the biogenesis of exosomes. *Nature Cell Biology*, *14*(7), 677–685. https://doi.org/10.1038/ncb2502

Bindels, D. S., Haarbosch, L., Van Weeren, L., Postma, M., Wiese, K. E., Mastop, M., … Gadella, T. W. J. (2016). MScarlet: A bright monomeric red fluorescent protein for cellular imaging. *Nature Methods*, *14*(1), 53–56. https://doi.org/10.1038/nmeth.4074

Böker, K. O., Lemus-Diaz, N., Rinaldi Ferreira, R., Schiller, L., Schneider, S., & Gruber, J. (2018). The Impact of the CD9 Tetraspanin on Lentivirus Infectivity and Exosome Secretion. *Molecular Therapy*, *26*(2), 634–647. https://doi.org/10.1016/j.ymthe.2017.11.008

CHARGAFF, E., & WEST, R. (1946). The biological significance of the thromboplastic protein of blood. *The Journal of Biological Chemistry*, *166*(1), 189–197. https://doi.org/10.1016/s0021-9258(17)34997-9

Chen, C., Sun, M., Wang, J., Su, L., Lin, J., & Yan, X. (2021). Active cargo loading into extracellular vesicles: Highlights the heterogeneous encapsulation behaviour. *Journal*

of Extracellular Vesicles, *10*(13). https://doi.org/10.1002/jev2.12163

Claire McGraw, Lewen Yang, Ilya Levental, Edward Lyman, and A. S.-R. (2019). Membrane Cholesterol Depletion Reduces Downstream Signaling Activity of the Adenosine A2a Receptor. *Biochim Biophys Acta Biomembr.*, *1861*(4), 760–767. https://doi.org/10.4049/jimmunol.1801473.The

Colombo, M., Moita, C., Van Niel, G., Kowal, J., Vigneron, J., Benaroch, P., … Raposo, G. (2013). Analysis of ESCRT functions in exosome biogenesis, composition and secretion highlights the heterogeneity of extracellular vesicles. *Journal of Cell Science*, *126*(24), 5553–5565. https://doi.org/10.1242/jcs.128868

Corso, G., Heusermann, W., Trojer, D., Görgens, A., Steib, E., Voshol, J., … Meisner-Kober, N. (2019). Systematic characterization of extracellular vesicles sorting domains and quantification at the single molecule–single vesicle level by fluorescence correlation spectroscopy and single particle imaging. *Journal of Extracellular Vesicles*, *8*(1). https://doi.org/10.1080/20013078.2019.1663043

Couch, Y., Buzàs, E. I., Vizio, D. Di, Gho, Y. S., Harrison, P., Hill, A. F., … Carter, D. R. F. (2021). A brief history of nearly EV-erything – The rise and rise of extracellular vesicles. *Journal of Extracellular Vesicles*, *10*(14). https://doi.org/10.1002/jev2.12144

Cranfill, P. J., Sell, B. R., Baird, M. A., Allen, J. R., Lavagnino, Z., De Gruiter, H. M., … Piston, D. W. (2016). Quantitative assessment of fluorescent proteins. *Nature Methods*, *13*(7), 557–562. https://doi.org/10.1038/nmeth.3891

Das, A., Goldstein, J. L., Anderson, D. D., Brown, M. S., & Radhakrishnan, A. (2013). Use of mutant 125I-Perfringolysin O to probe transport and organization of cholesterol in membranes of animal cells. *Proceedings of the National Academy of Sciences of the United States of America*, *110*(26), 10580–10585. https://doi.org/10.1073/pnas.1309273110

de Jong, O. G., Murphy, D. E., Mäger, I., Willms, E., Garcia-Guerra, A., Gitz-Francois, J.

J., … Vader, P. (2020). A CRISPR-Cas9-based reporter system for single-cell detection of extracellular vesicle-mediated functional transfer of RNA. *Nature Communications*, *11*(1), 1–13. https://doi.org/10.1038/s41467-020-14977-8

Del Conde, I., Shrimpton, C. N., Thiagarajan, P., & López, J. A. (2005). Tissue-factor-bearing microvesicles arise from lipid rafts and fuse with activated platelets to initiate coagulation. *Blood*, *106*(5), 1604–1611. https://doi.org/10.1182/blood-2004-03-1095

Denard, C. A., Paresi, C., Yaghi, R., McGinnis, N., Bennett, Z., Yi, L., … Iverson, B. L. (2021). YESS 2.0, a Tunable Platform for Enzyme Evolution, Yields Highly Active TEV Protease Variants. *ACS Synthetic Biology*, *10*(1), 63–71. https://doi.org/10.1021/acssynbio.0c00452

Dixon, A. S., Schwinn, M. K., Hall, M. P., Zimmerman, K., Otto, P., Lubben, T. H., … Wood, K. V. (2016). *NanoLuc Complementation Reporter Optimized for Accurate Measurement of Protein Interactions in Cells*. https://doi.org/10.1021/acschembio.5b00753

Dvorak, H. F., Quay, S. C., Orenstein, N. S., Dvorak, A. M., Hahn, P., Bitzer, A. M., & Carvalho, A. C. (1981). Tumor shedding and coagulation. *Science*, *212*(4497), 923–924. https://doi.org/10.1126/science.7195067

Dvorak, Harold F., Van Dewater, L., Dvorak, A. M., Harvey, V. S., Bitzer, A. M., Davis, G. L., … Carvalho, A. C. A. (1983). Procoagulant Activity Associated with Plasma Membrane Vesicles Shed by Cultured Tumor Cells. *Cancer Research*, *43*(9), 4434–4442.

Evans, B. C., Fletcher, R. B., Kilchrist, K. V., Dailing, E. A., Mukalel, A. J., Colazo, J. M., … Duvall, C. L. (2019). An anionic, endosome-escaping polymer to potentiate intracellular delivery of cationic peptides, biomacromolecules, and nanoparticles. *Nature Communications*, *10*(1). https://doi.org/10.1038/s41467-019-12906-y

Ferreira, J. V., Da Rosa Soares, A., Ramalho, J., Carvalho, C. M., Cardoso, M. H., Pintado,

P., … Pereira, P. (2022). LAMP2A regulates the loading of proteins into exosomes. *Science Advances*, *8*(12). https://doi.org/10.1126/sciadv.abm1140

Fu, S., Wang, Y., Xia, X., & Zheng, J. C. (2020a). Exosome engineering: Current progress in cargo loading and targeted delivery. *NanoImpact*, *20*(August), 100261. https://doi.org/10.1016/j.impact.2020.100261

Fu, S., Wang, Y., Xia, X., & Zheng, J. C. (2020b). Exosome engineering: Current progress in cargo loading and targeted delivery. *NanoImpact*, *20*(September), 100261. https://doi.org/10.1016/j.impact.2020.100261

Fuhrmann, G., Serio, A., Mazo, M., Nair, R., & Stevens, M. M. (2015). Active loading into extracellular vesicles significantly improves the cellular uptake and photodynamic effect of porphyrins. *Journal of Controlled Release*, *205*, 35–44. https://doi.org/10.1016/j.jconrel.2014.11.029

Gadella, T. W. J., van Weeren, L., Stouthamer, J., Hink, M. A., Wolters, A. H. G., Giepmans, B. N. G., … Royant, A. (2023). mScarlet3: a brilliant and fast-maturing red fluorescent protein. *Nature Methods*, *20*(April). https://doi.org/10.1038/s41592-023-01809-y

Goedhart, J., Von Stetten, D., Noirclerc-Savoye, M., Lelimousin, M., Joosen, L., Hink, M. A., … Royant, A. (2012). Structure-guided evolution of cyan fluorescent proteins towards a quantum yield of 93%. *Nature Communications*, *3*. https://doi.org/10.1038/ncomms1738

Gordón-Alonso, M., Yañez-Mó, M., Barreiro, O., Álvarez, S., Muñoz-Fernández, M. Á., Valenzuela-Fernández, A., & Sánchez-Madrid, F. (2006). Tetraspanins CD9 and CD81 Modulate HIV-1-Induced Membrane Fusion. *The Journal of Immunology*, *177*(8), 5129–5137. https://doi.org/10.4049/jimmunol.177.8.5129

Grove, J., & Marsh, M. (2011). The cell biology of receptor-mediated virus entry. *Journal of Cell Biology*, *195*(7), 1071–1082. https://doi.org/10.1083/jcb.201108131

Gupta, D., Liang, X., Pavlova, S., Wiklander, O. P. B., Corso, G., Zhao, Y., … EL Andaloussi, S. (2020). Quantification of extracellular vesicles in vitro and in vivo using sensitive bioluminescence imaging. *Journal of Extracellular Vesicles*, *9*(1). https://doi.org/10.1080/20013078.2020.1800222

Gurung, S., Perocheau, D., Touramanidou, L., & Baruteau, J. (2021). The exosome journey: from biogenesis to uptake and intracellular signalling. *Cell Communication and Signaling*, *19*(1), 1–19. https://doi.org/10.1186/s12964-021-00730-1

Han, C., & Qin, G. (2022). Reporter Systems for Assessments of Extracellular Vesicle Transfer. *Frontiers in Cardiovascular Medicine*, *9*(June), 1–6. https://doi.org/10.3389/fcvm.2022.922420

Hemler, M. E. (2003). Tetraspanin Proteins Mediate Cellular Penetration, Invasion, and Fusion Events and Define a Novel Type of Membrane Microdomain. *Annual Review of Cell and Developmental Biology*, *19*, 397–422. https://doi.org/10.1146/annurev.cellbio.19.111301.153609

Hemler, M. E. (2005). Tetraspanin functions and associated microdomains. *Nature Reviews Molecular Cell Biology*, *6*(10), 801–811. https://doi.org/10.1038/nrm1736

Heuck, A. P., Hotze, E. M., Tweten, R. K., & Johnson, A. E. (2000). Mechanism of membrane insertion of a multimeric β-barrel protein: Perfringolysin O creates a pore using ordered and coupled conformational changes. *Molecular Cell*, *6*(5), 1233–1242. https://doi.org/10.1016/S1097-2765(00)00119-2

Heusermann, W., Hean, J., Trojer, D., Steib, E., von Bueren, S., Graff-Meyer, A., … Meisner-Kober, N. C. (2016). Exosomes surf on filopodia to enter cells at endocytic hot spots, traffic within endosomes, and are targeted to the ER. *Journal of Cell Biology*, *213*(2), 173–184. https://doi.org/10.1083/jcb.201506084

Horibe, S., Tanahashi, T., Kawauchi, S., Murakami, Y., & Rikitake, Y. (2018). Mechanism of recipient cell-dependent differences in exosome uptake. *BMC Cancer*, *18*(1), 1–9.

https://doi.org/10.1186/s12885-017-3958-1

Horikawa, M., Sabe, H., & Onodera, Y. (2021). Strategies for all-at-once and stepwise selection of cells with multiple genetic manipulations. *Biochemical and Biophysical Research Communications, 582*, 93–99. https://doi.org/10.1016/j.bbrc.2021.10.016

Hoshino, A., Kim, H. S., Bojmar, L., Gyan, K. E., Cioffi, M., Hernandez, J., … Lyden, D. (2020). Extracellular Vesicle and Particle Biomarkers Define Multiple Human Cancers. *Cell*, *182*(4), 1044-1061.e18. https://doi.org/10.1016/j.cell.2020.07.009

Jimenez, R., Mukherjee, S., Hung, S. T., Douglas, N., Manna, P., Thomas, C., … Palmer, A. E. (2020). Engineering of a brighter variant of the fusionred fluorescent protein using lifetime flow cytometry and structure-guided mutations. *Biochemistry, 59*(39), 3669–3682. https://doi.org/10.1021/acs.biochem.0c00484

Johnson, B. B., Breña, M., Anguita, J., & Heuck, A. P. (2017). Mechanistic Insights into the Cholesterol-dependent Binding of Perfringolysin O-based Probes and Cell Membranes. *Scientific Reports*, *7*(1), 1–14. https://doi.org/10.1038/s41598-017-14002-x

Johnson, B. B., & Heuck, A. P. (2014). Perfringolysin O structure and mechanism of pore formation as a paradigm for cholesterol-dependent cytolysins. *Sub-Cellular Biochemistry*, *80*(413), 63–81. https://doi.org/10.1007/978-94-017-8881-6_5

Johnson, B. B., Moe, P. C., Wang, D., Rossi, K., Trigatti, B. L., & Heuck, A. P. (2012). Modifications in perfringolysin O domain 4 alter the cholesterol concentration threshold required for binding. *Biochemistry*, *51*(16), 3373–3382. https://doi.org/10.1021/bi3003132

Johnstone, R. M., Adam, M., Hammond, J. R., Orr, L., & Turbide, C. (1987). Vesicle formation during reticulocyte maturation. Association of plasma membrane activities with released vesicles (exosomes). *Journal of Biological Chemistry, 262*(19), 9412–9420. https://doi.org/10.1016/s0021-9258(18)48095-7

Joshi, B. S., de Beer, M. A., Giepmans, B. N. G., & Zuhorn, I. S. (2020). Endocytosis of Extracellular Vesicles and Release of Their Cargo from Endosomes. *ACS Nano*, *14*(4), 4444–4455. https://doi.org/10.1021/acsnano.9b10033

Kalluri, R., & LeBleu, V. S. (2020). The biology, function, and biomedical applications of exosomes. *Science*, *367*(6478). https://doi.org/10.1126/science.aau6977

Kicmal, T., Qing, E., Hawkins, G. M., Wilcox, A., & Gallagher, T. (2023). A cell-free platform to measure coronavirus membrane fusion. *STAR Protocols*, *4*(2), 102189. https://doi.org/10.1016/j.xpro.2023.102189

Kojima, R., Bojar, D., Rizzi, G., Hamri, G. C. El, El-Baba, M. D., Saxena, P., … Fussenegger, M. (2018). Designer exosomes produced by implanted cells intracerebrally deliver therapeutic cargo for Parkinson's disease treatment. *Nature Communications*, *9*(1). https://doi.org/10.1038/s41467-018-03733-8

Kotha, J., Longhurst, C., Appling, W., & Jennings, L. K. (2008). Tetraspanin CD9 regulates β1 integrin activation and enhances cell motility to fibronectin via a PI-3 kinase-dependent pathway. *Experimental Cell Research*, *314*(8), 1811–1822. https://doi.org/10.1016/j.yexcr.2008.01.024

Kulichkova, V. A., Selenina, A. V., Tomilin, A. N., & Tsimokha, A. S. (2018). Establishment of the HeLa Cell Line with Stable Expression of CD63 Exosome Marker Fused with Fluorescent Protein TagRFP and HTBH Tag. *Cell and Tissue Biology*, *12*(2), 146–152. https://doi.org/10.1134/S1990519X18020049

Kumar, G. A., & Chattopadhyay, A. (2016). Cholesterol: An evergreen molecule in biology. *Biomedical Spectroscopy and Imaging*, *5*(s1), S55–S66. https://doi.org/10.3233/bsi-160159

Kunkel, T. A. (1985). Rapid and efficient site-specific mutagenesis without phenotypic selection. *Proceedings of the National Academy of Sciences of the United States of America*, *82*(2), 488–492. https://doi.org/10.1073/pnas.82.2.488

KW, P., & Kierulf, B. (2015). Direct Isolation of Exosomes from Cell Culture: Simplifying Methods for Exosome Enrichment and Analysis. *Translational Biomedicine*, *6*(2), 1–9. https://doi.org/10.21767/2172-0479.100018

Lambert, T. J. (2019). FPbase: a community-editable fluorescent protein database. *Nature Methods*, *16*(4), 277–278. https://doi.org/10.1038/s41592-019-0352-8

Le Blanc, I., Luyet, P. P., Pons, V., Ferguson, C., Emans, N., Petiot, A., … Gruenberg, J. (2005). Endosome-to-cytosol transport of viral nucleocapsids. *Nature Cell Biology*, *7*(7), 653–664. https://doi.org/10.1038/ncb1269

Lin, Q., & London, E. (2013). Transmembrane protein (perfringolysin O) association with ordered membrane domains (rafts) depends upon the raft-associating properties of protein-bound Sterol. *Biophysical Journal*, *105*(12), 2733–2742. https://doi.org/10.1016/j.bpj.2013.11.002

Liu, S. L., Sheng, R., Jung, J. H., Wang, L., Stec, E., O'Connor, M. J., … Cho, W. (2017). Orthogonal lipid sensors identify transbilayer asymmetry of plasma membrane cholesterol. *Nature Chemical Biology*, *13*(3), 268–274. https://doi.org/10.1038/nchembio.2268

Llorente, A., Skotland, T., Sylvänne, T., Kauhanen, D., Róg, T., Orłowski, A., … Sandvig, K. (2013). Molecular lipidomics of exosomes released by PC-3 prostate cancer cells. *Biochimica et Biophysica Acta - Molecular and Cell Biology of Lipids*, *1831*(7), 1302–1309. https://doi.org/10.1016/j.bbalip.2013.04.011

Luan, X., Sansanaphongpricha, K., Myers, I., Chen, H., Yuan, H., & Sun, D. (2017). Engineering exosomes as refined biological nanoplatforms for drug delivery. *Acta Pharmacologica Sinica*, *38*(6), 754–763. https://doi.org/10.1038/aps.2017.12

Luby-Phelps, K. (2013). The physical chemistry of cytoplasm and its influence on cell function: An update. *Molecular Biology of the Cell*, *24*(17), 2593–2596. https://doi.org/10.1091/mbc.E12-08-0617

Maekawa, M. (2017). Domain 4 (D4) of perfringolysin O to visualize cholesterol in cellular membranes — The update. *Sensors (Switzerland)*, *17*(3), 1–14. https://doi.org/10.3390/s17030504

Maekawa, M., & Fairn, G. D. (2015). Complementary probes reveal that phosphatidylserine is required for the proper transbilayer distribution of cholesterol. *Journal of Cell Science*, *128*(7), 1422–1433. https://doi.org/10.1242/jcs.164715

Mathieu, M., Martin-Jaular, L., Lavieu, G., & Théry, C. (2019). Specificities of secretion and uptake of exosomes and other extracellular vesicles for cell-to-cell communication. *Nature Cell Biology*, *21*(1), 9–17. https://doi.org/10.1038/s41556-018-0250-9

Maxfield, F. R., & van Meer, G. (2010). Cholesterol, the central lipid of mammalian cells. *Current Opinion in Cell Biology*, *22*(4), 422–429. https://doi.org/10.1016/j.ceb.2010.05.004

Mehryab, F., Rabbani, S., Shahhosseini, S., Shekari, F., Fatahi, Y., Baharvand, H., & Haeri, A. (2020). Exosomes as a next-generation drug delivery system: An update on drug loading approaches, characterization, and clinical application challenges. *Acta Biomaterialia*, *113*, 42–62. https://doi.org/10.1016/j.actbio.2020.06.036

Merzlyak, E. M., Goedhart, J., Shcherbo, D., Bulina, M. E., Shcheglov, A. S., Fradkov, A. F., … Chudakov, D. M. (2007). Bright monomeric red fluorescent protein with an extended fluorescence lifetime. *Nature Methods*, *4*(7), 555–557. https://doi.org/10.1038/nmeth1062

Mesmin, B., & Maxfield, F. R. (2009). Intracellular sterol dynamics. *Biochimica et Biophysica Acta - Molecular and Cell Biology of Lipids*, *1791*(7), 636–645. https://doi.org/10.1016/j.bbalip.2009.03.002

Meyer, C., Losacco, J., Stickney, Z., Li, L., Marriott, G., & Lu, B. (2017). Pseudotyping exosomes for enhanced protein delivery in mammalian cells. *International Journal of*

Nanomedicine, *12*, 3153–3170. https://doi.org/10.2147/IJN.S133430

Miki, Y., Yashiro, M., Okuno, T., Kitayama, K., Masuda, G., Hirakawa, K., & Ohira, M. (2018). CD9-positive exosomes from cancerassociated fibroblasts stimulate the migration ability of scirrhous-type gastric cancer cells. *British Journal of Cancer*, *118*(6), 867–877. https://doi.org/10.1038/bjc.2017.487

Möbius, W., van Donselaar, E., Ohno-Iwashita, Y., Shimada, Y., Heijnen, H. F. G., Slot, J. W., & Geuze, H. J. (2003). Recycling compartments and the internal vesicles of multivesicular bodies harbor most of the cholesterol found in the endocytic pathway. *Traffic*, *4*(4), 222–231. https://doi.org/10.1034/j.1600-0854.2003.00072.x

Moe, P. C., & Heuck, A. P. (2010). Phospholipid hydrolysis caused by clostridium perfringens α-toxin facilitates the targeting of perfringolysin O to membrane bilayers. *Biochemistry*, *49*(44), 9498–9507. https://doi.org/10.1021/bi1013886

Molines, A. T., Lemière, J., Gazzola, M., Steinmark, I. E., Edrington, C. H., Hsu, C. T., … Chang, F. (2022). Physical properties of the cytoplasm modulate the rates of microtubule polymerization and depolymerization. *Developmental Cell*, *57*(4), 466-479.e6. https://doi.org/10.1016/j.devcel.2022.02.001

Moller-Tank, S., Kondratowicz, A. S., Davey, R. A., Rennert, P. D., & Maury, W. (2013). Role of the Phosphatidylserine Receptor TIM-1 in Enveloped-Virus Entry. *Journal of Virology*, *87*(15), 8327–8341. https://doi.org/10.1128/jvi.01025-13

Mulcahy, L. A., Pink, R. C., & Carter, D. R. F. (2014). Routes and mechanisms of extracellular vesicle uptake. *Journal of Extracellular Vesicles*, *3*(1). https://doi.org/10.3402/jev.v3.24641

Murate, M., & Kobayashi, T. (2016). Revisiting transbilayer distribution of lipids in the plasma membrane. *Chemistry and Physics of Lipids*, *194*, 58–71. https://doi.org/10.1016/j.chemphyslip.2015.08.009

Nelson, L. D., Johnson, A. E., & London, E. (2008). How interaction of perfringolysin O

with membranes is controlled by sterol structure, lipid structure, and physiological low pH: Insights into the origin of perfringolysin o-lipid raft interaction. *Journal of Biological Chemistry*, *283*(8), 4632–4642. https://doi.org/10.1074/jbc.M709483200

New, C., Lee, Z. Y., Tan, K. Sen, Wong, A. H. P., Wang, D. Y., & Tran, T. (2021). Tetraspanins: Host factors in viral infections. *International Journal of Molecular Sciences*, *22*(21), 1–21. https://doi.org/10.3390/ijms222111609

Nigri, J., Leca, J., Tubiana, S. S., Finetti, P., Guillaumond, F., Martinez, S., … Tomasini, R. (2022). CD9 mediates the uptake of extracellular vesicles from cancer-associated fibroblasts that promote pancreatic cancer cell aggressiveness. *Science Signaling*, *15*(745). https://doi.org/10.1126/scisignal.abg8191

O'Brien, D. K., & Melville, S. B. (2004). Effects of Clostridium perfringens alpha-toxin (PLC) and perfringolysin O (PFO) on cytotoxicity to macrophages, on escape from the phagosomes of macrophages, and on persistence of C. perfringens in host tissues. *Infection and Immunity*, *72*(9), 5204–5215. https://doi.org/10.1128/IAI.72.9.5204-5215.2004

O'Brien, K., Ughetto, S., Mahjoum, S., Nair, A. V., & Breakefield, X. O. (2022). Uptake, functionality, and re-release of extracellular vesicle-encapsulated cargo. *Cell Reports*, *39*(2), 110651. https://doi.org/10.1016/j.celrep.2022.110651

Ohmuro-Matsuyama, Y., Chung, C. I., & Ueda, H. (2013). Demonstration of protein-fragment complementation assay using purified firefly luciferase fragments. *BMC Biotechnology*, *13*. https://doi.org/10.1186/1472-6750-13-31

Ohno-Iwashita, Y., Iwamoto, M., Ando, S., & Iwashita, S. (1992). Effect of lipidic factors on membrane cholesterol topology - mode of binding of θ-toxin to cholesterol in liposomes. *BBA - Biomembranes*, *1109*(1), 81–90. https://doi.org/10.1016/0005-2736(92)90190-W

Onodera, Y., Nam, J. M., Horikawa, M., Shirato, H., & Sabe, H. (2018). Arf6-driven cell

invasion is intrinsically linked to TRAK1-mediated mitochondrial anterograde trafficking to avoid oxidative catastrophe. *Nature Communications*, *9*(1). https://doi.org/10.1038/s41467-018-05087-7

Osteikoetxea, X., Silva, A., Lázaro-Ibáñez, E., Salmond, N., Shatnyeva, O., Stein, J., … Dekker, N. (2022). Engineered Cas9 extracellular vesicles as a novel gene editing tool. *Journal of Extracellular Vesicles*, *11*(5). https://doi.org/10.1002/jev2.12225

Parmryd, S. M. and I. (2015). Cholesterol Depletion using Methyl-β-cyclodextrin. *Methods in Membrane Lipids*, *5*(8), 91–102.

Parolini, I., Federici, C., Raggi, C., Lugini, L., Palleschi, S., De Milito, A., … Fais, S. (2009). Microenvironmental pH is a key factor for exosome traffic in tumor cells. *Journal of Biological Chemistry*, *284*(49), 34211–34222. https://doi.org/10.1074/jbc.M109.041152

Peng, H., Ji, W., Zhao, R., Yang, J., Lu, Z., Li, Y., & Zhang, X. (2020). Exosome: a significant nano-scale drug delivery carrier. *Journal of Materials Chemistry B*, *8*(34), 7591–7608. https://doi.org/10.1039/d0tb01499k

Pfrieger, F. W., & Vitale, N. (2018). Thematic review series: Exosomes and microvesicles: Lipids as Key Components of their Biogenesis and Functions Cholesterol and the journey of extracellular vesicles. *Journal of Lipid Research*, *59*(12), 2255–2261. https://doi.org/10.1194/jlr.R084210

Prada, I., & Meldolesi, J. (2016). Binding and fusion of extracellular vesicles to the plasma membrane of their cell targets. *International Journal of Molecular Sciences*, *17*(8). https://doi.org/10.3390/ijms17081296

Ramachandran, R., Heuck, A. P., Tweten, R. K., & Johnson, A. E. (2002). Structural insights into the membrane-anchoring mechanism of a cholesterol-dependent cytolysin. *Nature Structural Biology*, *9*(11), 823–827. https://doi.org/10.1038/nsb855

Ratajczak, J., Miekus, K., Kucia, M., Zhang, J., Reca, R., Dvorak, P., & Ratajczak, M. Z.

(2006). Embryonic stem cell-derived microvesicles reprogram hematopoietic progenitors: Evidence for horizontal transfer of mRNA and protein delivery. *Leukemia*, *20*(5), 847–856. https://doi.org/10.1038/sj.leu.2404132

Santos, M. F., Rappa, G., Karbanová, J., Vanier, C., Morimoto, C., Corbeil, D., & Lorico, A. (2019). Anti-human CD9 antibody Fab fragment impairs the internalization of extracellular vesicles and the nuclear transfer of their cargo proteins. *Journal of Cellular and Molecular Medicine*, *23*(6), 4408–4421. https://doi.org/10.1111/jcmm.14334

Sarkisyan, K. S., Goryashchenko, A. S., Lidsky, P. V., Gorbachev, D. A., Bozhanova, N. G., Gorokhovatsky, A. Y., … Mishin, A. S. (2015). Green Fluorescent Protein with Anionic Tryptophan-Based Chromophore and Long Fluorescence Lifetime. *Biophysical Journal*, *109*(2), 380–389. https://doi.org/10.1016/j.bpj.2015.06.018

Shaner, N. C., Lin, M. Z., McKeown, M. R., Steinbach, P. A., Hazelwood, K. L., Davidson, M. W., & Tsien, R. Y. (2008). Improving the photostability of bright monomeric orange and red fluorescent proteins. *Nature Methods*, *5*(6), 545–551. https://doi.org/10.1038/nmeth.1209

Shimada, Y., Maruya, M., Iwashita, S., & Ohno-Iwashita, Y. (2002). The C-terminal domain of perfringolysin O is an essential cholesterol-binding unit targeting to cholesterol-rich microdomains. *European Journal of Biochemistry*, *269*(24), 6195–6203. https://doi.org/10.1046/j.1432-1033.2002.03338.x

Silva, A. M., Lázaro-Ibáñez, E., Gunnarsson, A., Dhande, A., Daaboul, G., Peacock, B., … Dekker, N. (2021). Quantification of protein cargo loading into engineered extracellular vesicles at single-vesicle and single-molecule resolution. *Journal of Extracellular Vesicles*, *10*(10). https://doi.org/10.1002/jev2.12130

Skog, J., Würdinger, T., van Rijn, S., Meijer, D. H., Gainche, L., Curry, W. T., … Breakefield, X. O. (2008). Glioblastoma microvesicles transport RNA and proteins that promote tumour growth and provide diagnostic biomarkers. *Nature Cell Biology*,

10(12), 1470–1476. https://doi.org/10.1038/ncb1800

Skotland, T., Hessvik, N. P., Sandvig, K., & Llorente, A. (2019). Exosomal lipid composition and the role of ether lipids and phosphoinositides in exosome biology. *Journal of Lipid Research*, *60*(1), 9–18. https://doi.org/10.1194/jlr.R084343

Somiya, M. (2020). Where does the cargo go?: Solutions to provide experimental support for the "extracellular vesicle cargo transfer hypothesis." *Journal of Cell Communication and Signaling*, *14*(2), 135–146. https://doi.org/10.1007/s12079-020-00552-9

Somiya, M., & Kuroda, S. (2021a). Real-Time Luminescence Assay for Cytoplasmic Cargo Delivery of Extracellular Vesicles. *Analytical Chemistry*, *93*(13), 5612–5620. https://doi.org/10.1021/acs.analchem.1c00339

Somiya, M., & Kuroda, S. (2021b). Reporter gene assay for membrane fusion of extracellular vesicles. *Journal of Extracellular Vesicles*, *10*(13). https://doi.org/10.1002/jev2.12171

Somiya, M., & Kuroda, S. (2022). Engineering of Extracellular Vesicles for Small Molecule-Regulated Cargo Loading and Cytoplasmic Delivery of Bioactive Proteins. *Molecular Pharmaceutics*. https://doi.org/10.1021/acs.molpharmaceut.2c00192

Sterzenbach, U., Putz, U., Low, L. H., Silke, J., Tan, S. S., & Howitt, J. (2017). Engineered Exosomes as Vehicles for Biologically Active Proteins. *Molecular Therapy*, *25*(6), 1269–1278. https://doi.org/10.1016/j.ymthe.2017.03.030

Sun, Z., Costell, M., & Fässler, R. (2019). Integrin activation by talin, kindlin and mechanical forces. *Nature Cell Biology*, *21*(1), 25–31. https://doi.org/10.1038/s41556-018-0234-9

Sung, B. H., von Lersner, A., Guerrero, J., Krystofiak, E. S., Inman, D., Pelletier, R., … Weaver, A. M. (2020). A live cell reporter of exosome secretion and uptake reveals pathfinding behavior of migrating cells. *Nature Communications*, *11*(1), 1–15.

https://doi.org/10.1038/s41467-020-15747-2

Teo, S. L. Y., Rennick, J. J., Yuen, D., Al-Wassiti, H., Johnston, A. P. R., & Pouton, C. W. (2021). Unravelling cytosolic delivery of cell penetrating peptides with a quantitative endosomal escape assay. *Nature Communications, 12*(1). https://doi.org/10.1038/s41467-021-23997-x

Théry, C., Witwer, K. W., Aikawa, E., Alcaraz, M. J., Anderson, J. D., Andriantsitohaina, R., … Zuba-Surma, E. K. (2018). Minimal information for studies of extracellular vesicles 2018 (MISEV2018): a position statement of the International Society for Extracellular Vesicles and update of the MISEV2014 guidelines. *Journal of Extracellular Vesicles*, *7*(1). https://doi.org/10.1080/20013078.2018.1535750

Thom, S. R., Bhopale, V. M., Yu, K., Huang, W., Kane, M. A., Margolis, D. J., & O'Neill, L. (2017). Neutrophil microparticle production and inflammasome activation by hyperglycemia due to cytoskeletal instability. *Journal of Biological Chemistry, 292*(44), 18312–18324. https://doi.org/10.1074/jbc.M117.802629

Tognoli, M. L., Dancourt, J., Bonsergent, E., Palmulli, R., de Jong, O. G., Van Niel, G., … Lavieu, G. (2023). Lack of involvement of CD63 and CD9 tetraspanins in the extracellular vesicle content delivery process. *Communications Biology*, *6*(1). https://doi.org/10.1038/s42003-023-04911-1

Tomabechi, Y., Hosoya, T., Ehara, H., Sekine, S. I., Shirouzu, M., & Inouye, S. (2016). Crystal structure of nanoKAZ: The mutated 19 kDa component of Oplophorus luciferase catalyzing the bioluminescent reaction with coelenterazine. *Biochemical and Biophysical Research Communications*, *470*(1), 88–93. https://doi.org/10.1016/j.bbrc.2015.12.123

Toribio, V., Morales, S., López-Martín, S., Cardeñes, B., Cabañas, C., & Yáñez-Mó, M. (2019). Development of a quantitative method to measure EV uptake. *Scientific Reports*, *9*(1), 1–14. https://doi.org/10.1038/s41598-019-47023-9

Trajkovic, K. (2008). Ceramide triggers budding of exosome vesicles into multivesicular endosomes (Science (1244)). *Science*, *320*(5873), 179. https://doi.org/10.1126/science.320.5873.179

Tsien, R. Y. (1998). The green fluorescent protein. *Annual Review of Biochemistry*, *67*, 509–544. https://doi.org/10.1146/annurev.biochem.67.1.509

Valadi, H., Ekström, K., Bossios, A., Sjöstrand, M., Lee, J. J., & Lötvall, J. O. (2007). Exosome-mediated transfer of mRNAs and microRNAs is a novel mechanism of genetic exchange between cells. *Nature Cell Biology*, *9*(6), 654–659. https://doi.org/10.1038/ncb1596

van Dongen, H. M., Masoumi, N., Witwer, K. W., & Pegtel, D. M. (2016). Extracellular Vesicles Exploit Viral Entry Routes for Cargo Delivery. *Microbiology and Molecular Biology Reviews*, *80*(2), 369–386. https://doi.org/10.1128/mmbr.00063-15

van Meer, G. (2011). Dynamic transbilayer lipid asymmetry. *Cold Spring Harbor Perspectives in Biology*, *3*(5), 1–11. https://doi.org/10.1101/cshperspect.a004671

van Niel, G., Charrin, S., Simoes, S., Romao, M., Rochin, L., Saftig, P., … Raposo, G. (2011). The Tetraspanin CD63 Regulates ESCRT-Independent and -Dependent Endosomal Sorting during Melanogenesis. *Developmental Cell*, *21*(4), 708–721. https://doi.org/10.1016/j.devcel.2011.08.019

Verherstraeten, S., Goossens, E., Valgaeren, B., Pardon, B., Timbermont, L., Haesebrouck, F., … Immerseel, F. Van. (2015). Perfringolysin o: The underrated clostridium perfringens toxin? *Toxins*, *7*(5), 1702–1721. https://doi.org/10.3390/toxins7051702

Votteler, J., Ogohara, C., Yi, S., Hsia, Y., Nattermann, U., Belnap, D. M., … Sundquist, W. I. (2016). Designed proteins induce the formation of nanocage-containing extracellular vesicles. *Nature*, *540*(7632), 292–295. https://doi.org/10.1038/nature20607

Wang, H. X., Li, Q., Sharma, C., Knoblich, K., & Hemler, M. E. (2011). Tetraspanin protein contributions to cancer. *Biochemical Society Transactions*, *39*(2), 547–552.

https://doi.org/10.1042/BST0390547

Wang, S., Ding, M., Xue, B., Hou, Y., & Sun, Y. (2018). Spying on protein interactions in living cells with reconstituted scarlet light. *Analyst*, *143*(21), 5161–5169. https://doi.org/10.1039/c8an01223g

Wiedenmann, J., Oswald, F., & Nienhaus, G. U. (2009). Fluorescent proteins for live cell imaging: Opportunities, limitations, and challenges. *IUBMB Life*, *61*(11), 1029–1042. https://doi.org/10.1002/iub.256

Witwer, K. W., Goberdhan, D. C. I., O'Driscoll, L., Théry, C., Welsh, J. A., Blenkiron, C., … Zheng, L. (2021). Updating MISEV: Evolving the minimal requirements for studies of extracellular vesicles. *Journal of Extracellular Vesicles*, *10*(14). https://doi.org/10.1002/jev2.12182

Yao, Z., Qiao, Y., Li, X., Chen, J., Ding, J., Bai, L., … Yuan, Z. (2018). Exosomes Exploit the Virus Entry Machinery and Pathway To Transmit Alpha Interferon-Induced Antiviral Activity. *Journal of Virology*, *92*(24). https://doi.org/10.1128/jvi.01578-18

Yusa, K., Zhou, L., Li, M. A., Bradley, A., & Craig, N. L. (2011). A hyperactive piggyBac transposase for mammalian applications. *Proceedings of the National Academy of Sciences of the United States of America*, *108*(4), 1531–1536. https://doi.org/10.1073/pnas.1008322108

Zeng, F., Zhang, S., Hao, Z., Duan, S., Meng, Y., Li, P., … Lin, Y. (2018). Efficient strategy for introducing large and multiple changes in plasmid DNA. *Scientific Reports*, *8*(1), 1–12. https://doi.org/10.1038/s41598-018-20169-8

Zhang, Q., Higginbotham, J. N., Jeppesen, D. K., Yang, Y. P., Li, W., McKinley, E. T., … Coffey, R. J. (2019). Transfer of Functional Cargo in Exomeres. *Cell Reports*, *27*(3), 940-954.e6. https://doi.org/10.1016/j.celrep.2019.01.009

Zitvogel L, Regnault A, Lozier A, Wolfers J, Flament C, Tenza D, Ricciardi-Castagnoli P, Raposo G, A. S., Zitvogel, L., Regnault, A., Lozier, A., Wolfers, J., Flament, C., …

Amigorena, S. (1998). Eradication of established murine tumors using a novel cell-free vaccine: dendritic cell-derived exosomes. *Nature Medicine*, *4*(5), 594–600. Retrieved from http://www.ncbi.nlm.nih.gov/pubmed/9585234%0Ahttp://www.nature.com/naturemedicine

Zomer, A., Maynard, C., Verweij, F. J., Kamermans, A., Schäfer, R., Beerling, E., … Van Rheenen, J. (2015). In vivo imaging reveals extracellular vesicle-mediated phenocopying of metastatic behavior. *Cell*, *161*(5), 1046–1057. https://doi.org/10.1016/j.cell.2015.04.042

Zomer, A., Steenbeek, S. C., Maynard, C., & Van Rheenen, J. (2016). Studying extracellular vesicle transfer by a Cre-loxP method. *Nature Protocols*, *11*(1), 87–101. https://doi.org/10.1038/nprot.2015.138